J. Fluid Mech. (1996), *vol.* 328, *pp.* 129–160

The instability and breakdown of tall columnar vortices in a quasi-geostrophic fluid

By DAVID G. DRITSCHEL[1]
AND MANUEL DE LA TORRE JUÁREZ[2]

[1]Department of Applied Mathematics and Theoretical Physics, University of Cambridge, Silver Street, Cambridge CB3 9EW, UK

[2]Departamento de Física Aplicada a la Ingeniería Aeronáutica, Universidad Politécnica de Madrid, Pza. Cardenal Cisneros 3, 28040 Madrid, Spain

(Received 2 November 1995 and in revised form 3 May 1996)

We examine the linear stability of elliptical columns of uniform potential vorticity subject to two-dimensional (horizontal) straining within a rapidly rotating, stratified (quasi-geostrophic) fluid. We find that horizontal straining can promote the exponential growth of three-dimensional disturbances when the vortex height-to-width aspect ratio exceeds, qualitatively, three times the ratio of the Coriolis parameter to the buoyancy frequency. This instability is *not* related to the usual baroclinic instability which operates on shallow vortex columns whose potential vorticity changes sign with height. The nonlinear development of these instabilities is investigated numerically using a high-resolution contour surgery algorithm. Simulations are conducted for both a Boussinesq (ocean-like) fluid and a compressible (atmospheric-like) fluid having exponentially decreasing density with height. The simulations reveal a generic nonlinear development that results in a semi-ellipsoidal baroclinic vortex dome at the lower surface and, in the case of a Boussinesq fluid, another such dome at the upper surface.

The related problem of two interacting vortex columns is also examined. A generic three-dimensional instability and nonlinear development occurs no matter how great the distance between the vortex columns, provided that they are sufficiently tall.

Our results may bear upon the observed structure of many atmospheric and oceanic vortices, whose height-to-width aspect ratios are consistent with our findings. Remarkably, even strongly ageostrophic vortices, such as tropical cyclones, fit the pattern. Our results furthermore re-open questions about the long-time nature of freely decaying quasi-geostrophic turbulence, for which recent simulations indicate a progressive two-dimensionalization by vortex alignment, while earlier simulations have indicated long-lived baroclinic vortices, not unlike what we find here.

1. Introduction

Coherent vortex structures play an important role in geophysical and astrophysical fluid dynamics. For example, the Earth's wintertime stratosphere is dominated by a huge vortex, called the 'polar vortex', having a radius of several thousand kilometres. It spins up as the pole cools at the onset of winter and is destroyed in early spring by a combination of solar heating and dynamical instabilities. In mid-winter, in the absence of solar heating, dissipation processes are weak and the vortex acquires a remarkably

steep edge gradient which permits it to be readily identified. The robustness of the stratospheric polar vortex is an issue of international concern because it bears strongly on ozone depletion (see McIntyre 1995 for a detailed account).

There are other important examples in ocean dynamics, e.g. surface-trapped eddies and the 'meddies' that are formed at mid-depth from the salt tongues issuing from the Mediterranean Sea or are spun off the major ocean fronts, such as the Gulf Stream and the Kuroshio Current, in the atmospheres of other planets, e.g. Jupiter's Great Red Spot, Venus' Polar Dipole and Neptune's Great Dark Spot, and almost certainly in astrophysical fluid dynamics, in the accretion discs of galaxies and solar systems. It is no wonder that vortex dynamics is a popular, intensively studied topic. Still, many questions remain.

One of the most important questions concerns the *three-dimensional structure* of such vortices. What controls this structure? A simple, perhaps unexpected answer is discovered here in an idealized model problem which, however, appears to be more generally applicable.

The simplest relevant model system is *quasi-geostrophic* vortex dynamics. Quasi-geostrophy is a useful, commonly employed approximation valid for a rapidly rotating, stratified fluid (for a general description see Pedlosky 1979 and Houghton 1986; for a mathematical discussion, see Stegner & Zeitlin 1995; for 'contour dynamics' and an application to the stratospheric polar vortex, see Dritschel & Saravanan 1994). The real simplifying feature of quasi-geostrophy is the omission of high-speed gravity waves. Additionally, there exists a linear-operator relationship between the quasi-geostrophic (QG) potential vorticity (hereafter PV) and the streamfunction, from which one can deduce all properties of the flow (i.e. the velocity and the (potential) temperature or density field) – this is the so-called 'invertibility principle' (Hoskins, McIntyre & Robertson).

We study here the three-dimensional linear stability and nonlinear evolution of two-dimensional *columnar* vortices containing *uniform* PV. Such vortices are the simplest one may consider, since stability or instability is decided purely from the dynamics of the vortex boundary (a two-dimensional surface). We examine, in particular, elliptical vortices, columns of uniform PV having an elliptical cross section. Elliptical vortices are the structures most frequently found in high-Reynolds-number two-dimensional flows; inevitably, vortices are subject to external strain due to the surrounding flow field, which, to leading order, appears locally as an incompressible, irrotational linear velocity field and which deforms vortices into elliptical shapes. An elliptical vortex remains elliptical in such a flow – this result is due to Moore & Saffman (1971) and Kida (1981) and has been exploited extensively in simplified models of two-dimensional vortex dynamics by Melander, Zabusky & Stycek (1986) and Legras & Dritschel (1991). An ellipse possesses the advantage of being, together with the circle, the simplest two-dimensional equilibrium shape. Little is known, however, about the stability of vortex columns of this or any other shape; even the two-dimensional stability problem is not well understood. We do know that a circular column is stable to finite-amplitude disturbances as a consequence of angular momentum conservation (Dritschel 1988), but no such result is available for an elliptical column.

Much is known about the linear stability of the elliptical vortex. After Kirchhoff (1876) demonstrated that a uniform elliptical vortex rotates uniformly without change of shape, Love (1893) determined that such a vortex is linearly unstable (to two-dimensional disturbances) if its aspect ratio is less than $\frac{1}{3}$. At this aspect ratio, an instability with three-fold symmetry erupts, which is followed by one with four-fold symmetry at a yet smaller aspect ratio, etc. In the nonlinear regime, the vortex casts

off tongues of vorticity and, after a complex period of filamentation, a nearly elliptical vortex re-emerges (Dritschel 1986).

Recently, Miyazaki & Hanazaki (1994) investigated the linear three-dimensional QG stability of Kirchhoff's (freely rotating) elliptical vortex. Their results form a basis for the present study and are reviewed and elaborated below in §2. They showed that an elliptical vortex, even of small eccentricity, can be unstable both to a long-(vertical) wavelength twisting disturbance and to an intermediate-wavelength tilting disturbance. We say 'can be' since, in practice, the vertical extent of the fluid is confined, restricting both the set of possible disturbance wavelengths and the length of the longest wave. These instabilities intensify with decreasing vortex aspect ratio without the appearance of new modes of instability until the aspect ratio is less than about $\frac{1}{3}$, when instabilities of two-dimensional origin are encountered (details can be found below in §2).

An apparently similar instability operating on ellipsoids of uniform PV in a Boussinesq QG fluid, unbounded horizontally and vertically, was uncovered earlier by Meacham (1992). He concluded that sufficiently tall vortices must be nearly circular to be stable, consistent with the results of Miyazaki & Hanazaki (1994). The nonlinear development of this instability on tall vortices was not investigated.

The case of an elliptical vortex column in an external straining flow is considerably more complicated. The two-dimensional stability alone is a formidable problem (Dritschel 1990) and, to simplify matters, we here restrict our attention to the *steady* (non-oscillating) elliptical vortices, for which there is a relationship between the vortex aspect ratio and the external strain flow parameters. (Under slowly changing external conditions, vortices are frequently observed to pass through a series of near-equilibrium states – see Legras & Dritschel (1993) and Dritschel (1995).) The linear two-dimensional stability of these vortices depends on two parameters and is reviewed in §2.2 (the freely rotating elliptical vortex is included as a special case). By considering the linear three-dimensional stability, as we do in §§2.3 and 2.4, we are adding one more parameter, the disturbance's vertical wavenumber, and the amount of numerical computation necessary to map out just the linear stability is staggering.

The complementary problem of the linear three-dimensional stability of a strained elliptical vortex in an *unstratified* fluid was recently examined by Bayly, Holm & Lifschitz (1995). They used the method of geometrical optics to determine extensive domains of instability to high-wavenumber (small-scale) disturbances. (The freely rotating case has been studied without restriction to high wavenumbers by Miyazaki, Imai & Fukumoto 1995.) This instability appears to be fundamentally different from that examined in the present work; we have found that the presence of stratification stabilizes high-wavenumber disturbances.

Linear stability is only part of the problem. Given that there are unstable regions in the parameter space, a complete treatment of the problem requires an examination of the nonlinear evolution. What does an unstable basic state do; where does it go? The answer may help to understand what controls the structure of vortices. In §3 of this paper, we exhibit the development of a variety of unstable flows, contrasting a Boussinesq, uniform-density fluid with a compressible, exponentially decreasing-density fluid. It is discovered that a single type of three-dimensional structure emerges.

The results found for steady-strained ellipses in this paper can be used to draw conclusions concerning the three-dimensional stability of two well-separated columns of vorticity. This is done in §4 for two columns of like-signed and opposite-signed PV in a Boussinesq fluid, and some numerical simulations are performed for illustration.

We conclude in §5 by showing how our results may explain the observed structure of atmospheric and oceanic vortices. In this context, we outline a number of applied research problems stemming from the present results. We also discuss the implications of our results for QG turbulence. The persistence of three-dimensional structures, we argue, requires much weaker dissipation than presently employed by conventional numerical models.

2. Linear stability

2.1. *Basic problem formulation*

The equations governing quasi-geostrophic flow (see Hoskins *et al.* 1985, §5(b)) are

$$\frac{\mathrm{D}q}{\mathrm{D}t} \equiv \frac{\partial q}{\partial t} + \boldsymbol{u} \cdot \nabla_h q = 0, \tag{1a}$$

$$\nabla_h^2 \psi + \frac{1}{\rho_0} \frac{\partial}{\partial z} \left(\rho_0 \frac{f_0^2}{N^2} \frac{\partial \psi}{\partial z} \right) = q - f, \tag{1b}$$

$$\frac{\partial \psi}{\partial z} = 0 \quad \text{at} \quad z = 0 \quad \text{and} \quad H, \tag{1c}$$

$$u = -\frac{\partial \psi}{\partial y} \quad \text{and} \quad v = \frac{\partial \psi}{\partial x}, \tag{1d}$$

where $q(x, y, z, t)$ is the QG potential vorticity (PV), f is the Coriolis parameter (twice the planetary angular velocity projected normal to the planet's surface), f_0 is a reference value of f, ∇_h^2 is the horizontal Laplace operator, ψ is the streamfunction (proportional to the perturbation geopotential), $\boldsymbol{u} \equiv (u, v)$ is the horizontal velocity (there is no vertical advection of q), $\rho_0(z)$ is the basic-state density profile with height z (actually, z is log-pressure, the fluid being in hydrostatic equilibrium), and $N(z)$ is the buoyancy frequency of a neutral particle undergoing vertical oscillations. In this paper, we restrict the analysis to constant f, that is $f = f_0$, and henceforth absorb f into q. The problem is considerably more difficult for variable f (e.g. a β-plane) due to the inherent unsteadiness of the basic state (see e.g. Sutyrin *et al.* 1994), though a recent numerical breakthrough has made it accessible at least to direct numerical simulation (Dritschel & Ambaum 1996).

The basic state is a (height-independent) elliptical column

$$\frac{x^2}{a^2} + \frac{y^2}{b^2} = 1$$

of uniform PV, $q = 1$, bounded between two rigid surfaces at $z = 0$ and H, and immersed in a background two-dimensional straining flow of the general form

$$u_{ext} = (\gamma + \Omega) y \quad \text{and} \quad v_{ext} = (\gamma - \Omega) x \tag{2}$$

where γ is the strain rate (or deformation rate) and Ω is the background rotation, or, more appropriately, the rotation rate of the strain axes (we have adopted a frame of reference in which these axes are fixed; in this frame, q is supplemented by -2Ω everywhere). This straining flow is the same at all heights z.

Any three-dimensional solution may be written as a superposition of linearly independent vertical modes, arising from the separability of the horizontal and

vertical parts of the 'inversion operator' in (1*b*); that is, putting

$$\psi(x, y, z, t) = \sum_{n=0}^{\infty} \psi_n(x, y, t)\varphi_n(z) \tag{3}$$

with

$$\frac{1}{\rho_0}\frac{\mathrm{d}}{\mathrm{d}z}\left(\rho_0 \frac{f^2}{N^2}\frac{\mathrm{d}\varphi_n}{\mathrm{d}z}\right) + \alpha_n^2\varphi_n = 0, \qquad \frac{\mathrm{d}\varphi_n}{\mathrm{d}z} = 0 \ \text{ at } \ z = 0,\ H, \tag{4a}$$

where the $\alpha_n^2 \geqslant 0$ are the separation constants, one arrives at a series of two-dimensional problems, one for each n:

$$\nabla_h^2\psi_n - \alpha_n^2\psi_n = q_n, \tag{4b}$$

where $q_n(x, y, t)$ is the projection of the PV onto the nth vertical mode. Here, $1/\alpha_n$ is often referred to the 'internal radius of deformation' for mode n. By virtue of the boundary conditions at $z = 0$ and H, it is always true that $\alpha_0 = 0$ (this would not be true if the fluid had a free surface; moreover, the basic state would no longer be a precisely elliptical column). The vertically uniform basic state with $q = q_0 = 1 - 2\Omega$ $\forall z$ has

$$\psi = \psi_0(x, y) = \frac{1}{2(a+b)}(bx^2 + ay^2) + \tfrac{1}{2}[(\gamma - \Omega)x^2 - (\gamma + \Omega)y^2]$$

inside the vortex. Any disturbed state is generally a sum of this basic state and a perturbation of the form (3). The perturbation imparts three-dimensionality, which may be enhanced through dynamical instability.

In the absence of disturbances, the vortex will remain an elliptical column (Kida 1981), (the flow is then two-dimensional), though it will generally exhibit unsteady motion unless its major axis is aligned with the x-axis *and* Ω is chosen as a specific function of γ and the vortex cross-sectional aspect ratio $\lambda \equiv b/a \leqslant 1$, namely

$$\Omega = \frac{\lambda}{(1+\lambda)^2} + \gamma\frac{1+\lambda^2}{1-\lambda^2} \tag{5}$$

– this makes ψ a constant on the boundary of the vortex (Moore & Saffman 1971). We consider only these steady basic states in this paper.

Linear stability is examined by subjecting the vortex boundary to infinitesimal three-dimensional disturbances. Such disturbances arise naturally as a result of heterogeneities in the external flow field, and are sufficient to describe any exponentially amplifying mode of instability.

We can now examine linear stability, mode by mode, via a series of two-dimensional problems, in each of which the projected PV, q_n, is a two-dimensional displacement of an elliptical contour. The procedure is essentially identical to that used to examine purely two-dimensional stability, described in Appendix B of Dritschel (1995), the only difference being that the two-dimensional disturbance inversion operator is $\nabla_h^2 - \alpha_n^2$ instead of just ∇_h^2. This entails using the Green function $-K_0(\alpha_n r)$ in place of $\log r$, where r is two-dimensional distance, in the disturbance evolution equation, equation (B2*b*) of Dritschel (1995).

For the sake of clarity, the procedure is briefly outlined here. The equilibrium boundary of the patch, $\boldsymbol{x}_e(\theta) = (a\cos\theta, b\sin\theta)$ is disturbed to

$$\boldsymbol{x}(\theta, t) = \boldsymbol{x}_e(\theta) + \eta(\theta, t)\frac{\{\mathrm{d}y_e/\mathrm{d}\theta, -\mathrm{d}x_e/\mathrm{d}\theta\}}{(\mathrm{d}x_e/\mathrm{d}\theta)^2 + (\mathrm{d}y_e/\mathrm{d}\theta)^2}$$

where $\eta(\theta, t)$ is a scalar disturbance function (a displacement normal to the equilibrium vortex boundary). This function satisfies

$$\frac{\partial \eta}{\partial t} + \Omega_e \frac{\partial \eta}{\partial \theta} = \frac{q}{2\pi} \frac{\partial}{\partial \theta} \int_0^{2\pi} \eta(\theta', t) K_0(k|\boldsymbol{x}_e(\theta) - \boldsymbol{x}_e(\theta')|) \mathrm{d}\theta'$$

where q is the PV inside the vortex (unity here) and where we have put $\alpha_n = k$ in the argument of K_0; *we will subsequently refer to k as the vertical wavenumber of the disturbance*, even though it corresponds to a sinusoidal disturbance only when both N and ρ_0 are constant. In this formula, $\Omega_e = \mathrm{d}\theta/\mathrm{d}t$ along the equilibrium boundary; Ω_e is independent of θ for the elliptical basic state used here, and satisfies

$$\begin{aligned} \Omega_e &= (1 - 2\Omega) \frac{\lambda}{1 + \lambda^2} \\ &= \frac{\lambda}{(1 + \lambda)^2} - \frac{2\gamma\lambda}{1 - \lambda^2}. \end{aligned}$$

The disturbance function is expanded in a truncated sum of sinusoidal functions of θ multiplied by an exponential time factor:

$$\eta(\theta, t) = \mathrm{e}^{-\mathrm{i}\sigma t} \sum_{m=1}^{M} A_m \cos m\theta + B_m \sin m\theta$$

where σ is generally complex, the imaginary part of which, if positive, indicates exponential disturbance growth and hence linear instability. Both σ and the amplitudes A_m and B_m are determined numerically using a matrix-eigenvalue method. A truncation of $M = 20$ was found to give at least three decimal place accuracy except for $\lambda \ll 1$ and $k \gg 1$.

2.2. *Two-dimensional stability*

For $k = 0$ (the two-dimensional stability), there is no coupling between different m modes, and one can derive the stability results analytically (Moore & Saffman 1971; Dritschel 1990):

$$\sigma_m = \pm \left[\left(m\Omega_e - \tfrac{1}{2} \right)^2 - \frac{1}{4} \left(\frac{1 - \lambda}{1 + \lambda} \right)^{2m} \right]^{1/2} \tag{6}$$

– the growth rates ($\mathrm{Im}(\sigma_m) \equiv \sigma_i$) are plotted in figure 1(*a*) as a function of γ and λ; figure 1(*b*) shows the corresponding background rotation rate Ω, from (5). An alternative view of the instability growth rates is given in figure 1(*c*, *d*), which shows $\sigma_i(\Omega, \gamma)$ for $kR = 0$ in two distinct parts of the parameter space, differentiated by the sign of $\partial\lambda/\partial\gamma$. No such fold in parameter space occurs when using γ and λ as independent parameters.

The results for $\gamma = 0$ (no strain) were obtained by Love (1893) and can be found along the vertical line dividing figure 1(*a*) in half; one sees the $m = 3$ instability for $\lambda < \frac{1}{3}$ followed by $m = 4$, etc., for decreasing λ. For γ slightly negative, one encounters the $m = 2$ instability tongue, but the instabilities there lead only to vacillation (the vortex latches on to a periodic, pulsating solution which is still an elliptical vortex; Kida (1981), Dritschel (1990)). The tongue associated with $m = 1$ is irrelevant for the strictly two-dimensional vortex; $m = 1$ corresponds to a displacement of the vortex, which grows exponentially at the rate $(\gamma^2 - \Omega^2)^{1/2}$ when $|\gamma| > |\Omega|$. It is not irrelevant for $k > 0$ as we will see shortly. There are no instabilities for $\Omega > \frac{1}{2}$ (notably the PV

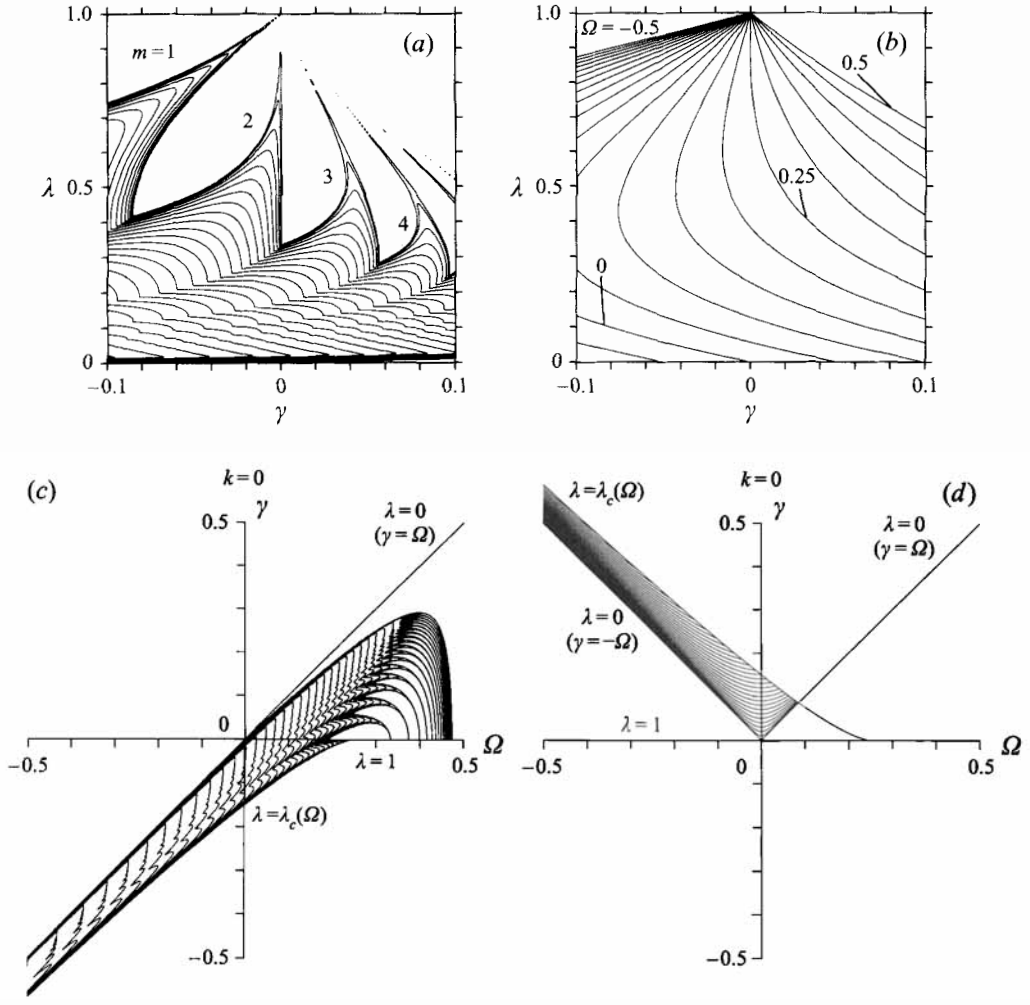

FIGURE 1. (*a*) Growth rates $\sigma_i(\gamma, \lambda)$ of two-dimensional disturbances to an elliptical vortex column. The contour interval is $\Delta\sigma_i = 0.01$ and the minimum level shown is $\sigma_{min} = 0.0001$. This contouring scheme is used in all subsequent growth rate maps. (*b*) Equilibrium angular velocity $\Omega(\gamma, \lambda)$ corresponding to (*a*). $\Delta\Omega = 0.05$ and $\Omega \in [-\frac{1}{2}, \frac{1}{2}]$. (*c*, *d*) Growth rates, as in (*a*), but now plotted as a function of Ω and γ, in two distinct parts of the folded parameter space; (*c*) shows $\sigma_i(\Omega, \gamma)$ when $\partial\lambda/\partial\gamma < 0$, and (*d*) shows $\sigma_i(\Omega, \gamma)$ when $\partial\lambda/\partial\gamma > 0$.

is then everywhere negative). Broadly speaking, vortices with small eccentricity are two-dimensionally stable.

2.3. *Three-dimensional stability of a freely rotating ellipse*

For $k > 0$ (the three-dimensional stability), different m modes in general couple, with a strength that grows with increasing k. In this subsection, we review the results for $\gamma = 0$, first obtained by Miyazaki & Hanazaki (1994). We have reproduced their results quantitatively using a different numerical solution method, and the growth rates obtained are plotted in figure 2 as a function of kR and λ, where $R = (ab)^{1/2}$ is the mean radius of the vortex. Their surprising result, which motivated our study, is indicated by the two tongues of instability emanating from the $\lambda = 1$ axis (where the vortex is circular, and stable) at $kR = 0$ and $kR \simeq 1.7046$. These are both three-

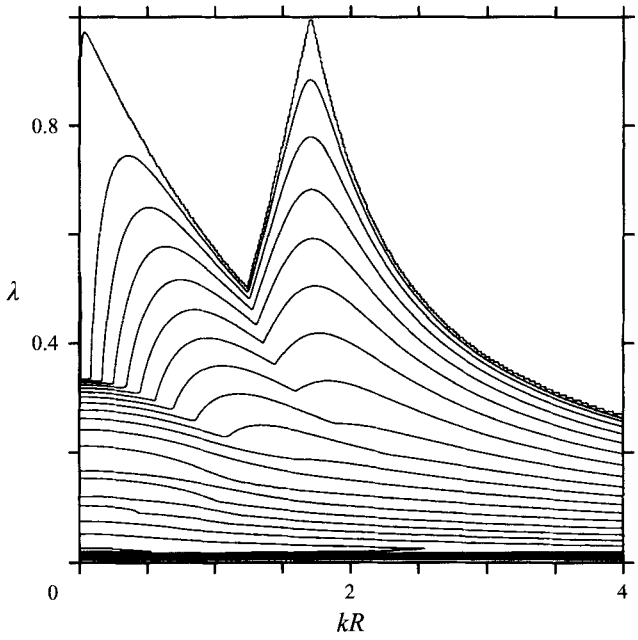

FIGURE 2. Growth rates $\sigma_i(kR, \lambda)$ of three-dimensional disturbances to a freely rotating elliptical column (i.e. $\gamma = 0$).

dimensional instabilities, and are distinct from the one of two-dimensional origin seen emerging from the $kR = 0$ axis when $\lambda < \frac{1}{3}$.

The intermediate-wavelength instability is odd, involving primarily $m = 1$, and thus would be seen as a displacement of the axis of the column by an amount proportional to the associated vertical mode, $\varphi_n(z)$, *if the mean radius R of the vortex column is such as to allow* $\alpha_n R$ *to be in the range of instability.* The long-wavelength instability is even, involving primarily $m = 2$. It would be seen as a twisting of the vortex column, since the disturbance in each plane is out of phase with the basic elliptical shape (Miyazaki & Hanazaki 1994). This long-wave instability connects with the $m = 2$ stability tongue bordering $\gamma = 0$ in figure 1(*a*). The connection of the intermediate-wavelength instability to the $m = 1$ tongue in figure 1(*a*) is less evident, but it will be demonstrated below. Note that the intermediate-wavelength instability has higher growth rates than the long-wave one for $\lambda \gtrsim 0.4$.

It is noteworthy that no reference has been made to particular horizontal or vertical scales; these instabilities afflict columns of particular height-to-width aspect ratios, fixed by the dimensionless number kR. For a Boussinesq, constant-N fluid, k is restricted to one of the α_n, given by $n\pi f/NH$, $n = 0, 1, 2, \ldots$. The combination NH/f is often called the 'Rossby radius of deformation' L_R, and in terms of L_R, we have $kR = n\pi R/L_R$, showing that R must be small compared with L_R, especially for the long-wavelength instability. In terms of the vortex height-to-width aspect ratio, we have $H/2R = (n\pi/2kR)(f/N)$, showing that the column must be tall on the scale of Prandtl's ratio, f/N, the natural vertical-to-horizontal ratio appearing in the QG equations, cf. (1*b*).

Some predictions for the nonlinear development of these instabilities were made by Miyazaki & Hanazaki (1994), who argued that the conservation of angular impulse used to prove the finite-amplitude stability of a *circular* column in a three-dimensional

QG fluid (Dritschel 1988) would ultimately limit the growth of disturbances to an *elliptical* column (this is verified below in §3). One might be tempted to conclude that their newly found instability is then of little consequence. Our interest grew from the recognition that, in the presence of external strain, angular impulse is no longer conserved and thus cannot be used to prove finite-amplitude stability for *any* basic state. The presence of strain, however weak, fundamentally alters the problem.

2.4. *Three-dimensional stability of a steady, strained ellipse*

We now display the results for various weak values of the strain rate, γ. Results for $\gamma = \pm 0.001$, ± 0.02 and ± 0.05 are displayed in figure 3(*a–f*). This figure rises out of figure 1(*a*), for $k = 0$, along lines of constant γ. For small positive γ, figure 3(*b*), the instability tongues are displaced to the right (shorter waves), particularly their tips near $\lambda = 1$ (compare with figure 2 for $\gamma = 0$). In fact, complete stabilization occurs for $\lambda > (1 - 2\gamma)/(1 + 2\gamma)$, i.e. when $\Omega \geqslant \frac{1}{2}$. For small negative γ, figure 3(*a*), the instability tongues are displaced to the left (longer waves). In particular, the intermediate-wavelength tongue on the right turns sharply toward the $k = 0$ axis and connects to the $m = 1$ tongue in figure 1(*a*). This displacement to the left or to the right increases with increasing $|\gamma|$. For $\gamma < 0$, the instabilities intensify while being displaced downward in λ, but no new modes of instability appear (the upper tongue always emerges from the $m = 1$ tongue for $k = 0$). For $\gamma > 0$, the instabilities diminish while also being displaced downward in λ, and in this case new tongues appear, emerging from tongues having $m > 2$ when $k = 0$. One can see the origin of these tongues on the right-hand side of figure 1(*a*). In figure 3(*f*), for example, one can see a trace of the $m = 4$ tongue emerging from $k = 0$, and then, from left to right along the bottom, $m = 3$, $m = 2$ and $m = 1$; however, these instabilities may develop only on highly eccentric (small λ) vortices.

An orthogonal view of the results is given in figure 4(*a–c*), in which λ is held fixed while γ and kR are varied (the results in figure 4(*c*) are used to initialize the nonlinear simulations in the following section). As λ approaches 1, the region of instability shrinks rapidly and the growth rates diminish, leaving the tongue of $m = 1$ origin as the only significant instability.

In summary, elliptical vortices close to a circular form ($\lambda \gtrsim \frac{1}{2}$) are maximally unstable to a disturbance largely consisting of a displacement mode ($m = 1$), which is manifested as a tilting of the vortex column. The column must however be tall enough, or narrow enough, to accommodate the vertical structure of the disturbance.

3. Nonlinear evolution

The linear stability analysis presented above helps to delineate the region of parameter space where three-dimensional development may occur. But the significance of this instability cannot be assessed without direct numerical simulation using the nonlinear equations. We have performed many such simulations in the two distinct parts of parameter space shown in figures 1(*c*) and 1(*d*). Remarkably, we have found little qualitative difference between the two parts of parameter space, despite their different origins.

3.1. *Numerics and initialization*

The PV distribution being piecewise uniform, contour dynamics affords the simplest means of exploring the nonlinear development of the instabilities described above. High-resolution simulations are conducted using the multi-layer/level QG contour

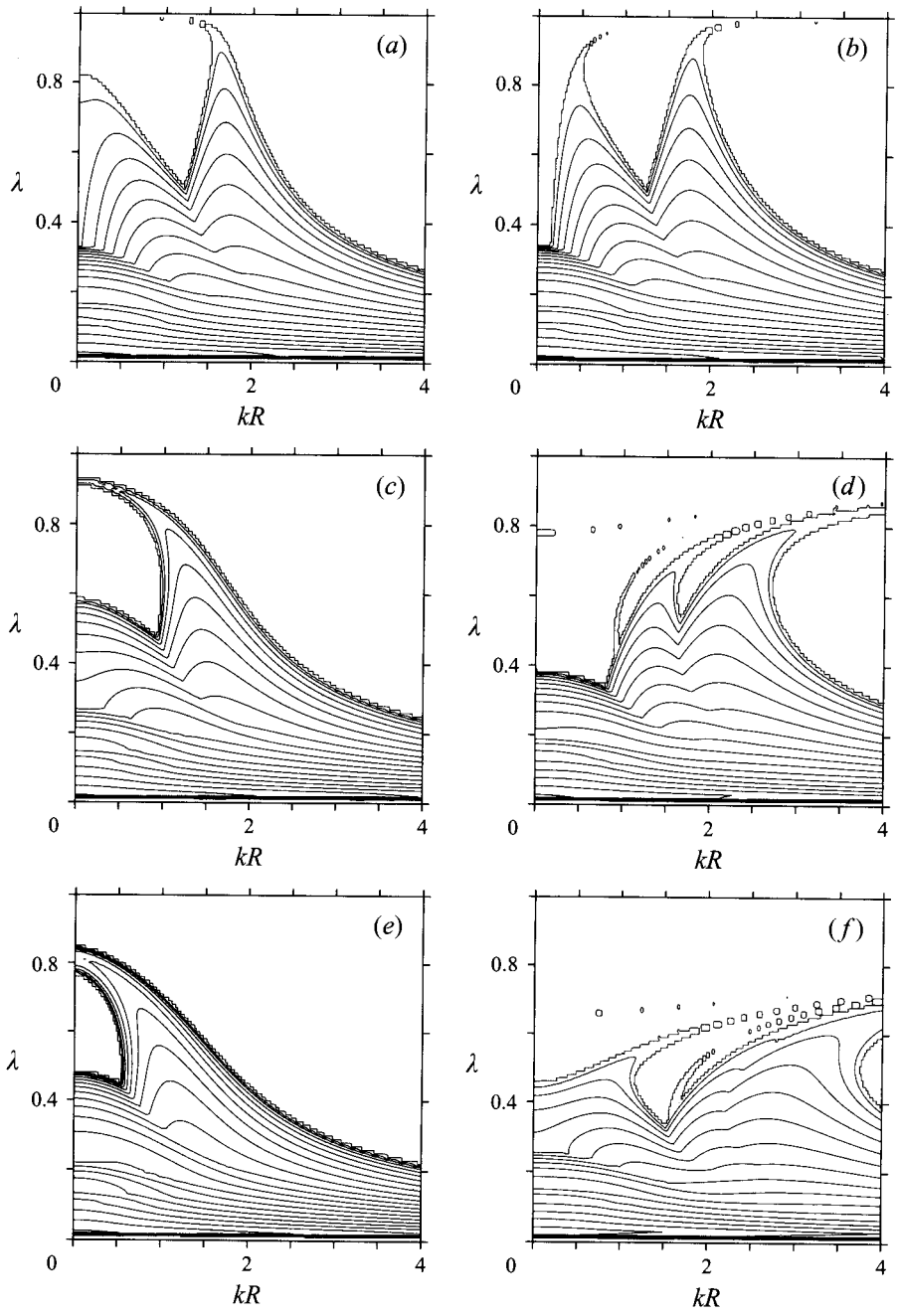

FIGURE 3. Growth rates $\sigma_i(kR, \lambda)$ of three-dimensional disturbances to a strained elliptical column. (*a*) $\gamma = -0.001$, (*b*) $\gamma = +0.001$, (*c*) $\gamma = -0.02$, (*d*) $\gamma = +0.02$, (*e*) $\gamma = -0.05$ and (*f*) $\gamma = +0.05$.

surgery algorithm developed by Dritschel & Saravanan (1994). 'Contour surgery' is the name given to the numerically-refined version of 'contour dynamics' having an automatic, controlled and well-tested means of removing fine-scale filamentary vorticity (see Dritschel 1989 for details).

Simulations are performed for two basic types of density stratification: (i) Boussinesq (uniform mean density) and (ii) compressible (exponentially decreasing density

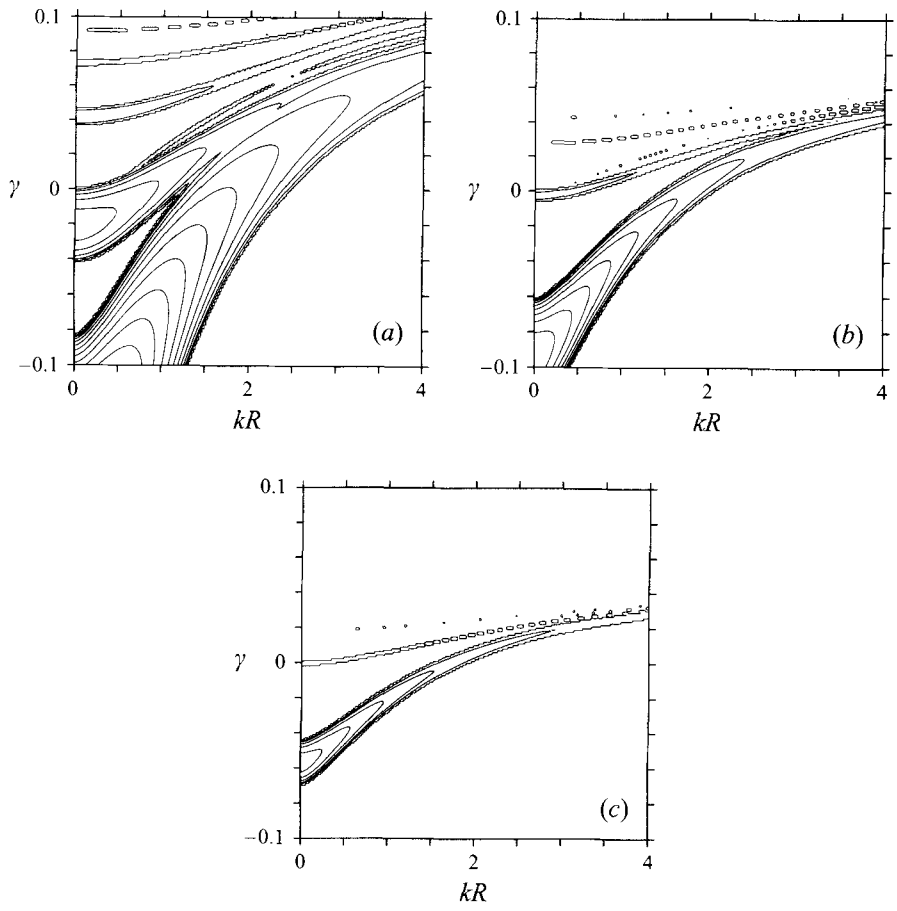

FIGURE 4. Growth rates $\sigma_i(kR, \gamma)$ of three-dimensional disturbances to a strained elliptical column. (*a*) $\lambda = 0.5$, (*b*) $\lambda = 0.7$ and (*c*) $\lambda = 0.8$.

with height). In both cases, a constant buoyancy frequency N is taken for simplicity. The first case is often taken to model the ocean and the second the stratosphere. Full details of these cases, the basic equations, and the numerics for the QG code may be found in Dritschel & Saravanan (1994).

In each case, the flow is bounded vertically by two rigid, horizontal planes. As discussed in §2, this gives rise to a discrete spectrum of vertical wavenumbers k (given below), and thus in practice the stability of the vortex depends on the boundaries and on the basic density stratification.

In the Boussinesq case, the basic height scale is taken to be the depth of the domain, H, while in the compressible case, it is taken to be a 'density scale-height', i.e. the basic density in this case is $\rho_0(z) = \rho_{0s}\exp(-z/H)$, where ρ_{0s} is the density at the bottom of the domain, $z = 0$. The vertical extent of the domain in the compressible case is limited to cH, with $c = 5.86$, to mimic typical stratospheric conditions (Dritschel & Saravanan 1994). Note that the natural horizontal scale is $L_R = NH/f$.

For the Boussinesq case,

$$\varphi_n(z) = \cos\alpha_n z\,; \quad \alpha_n = \frac{n\pi}{L_R}, \tag{7}$$

while for the compressible case,

$$\varphi_n(z) = \mathrm{e}^{z/2H}\mathrm{Re}\left[\left(\frac{2n\pi}{c} + \mathrm{i}\right)\mathrm{e}^{\mathrm{i}n\pi z/cH}\right]; \quad \alpha_n = \frac{1}{L_R}\left[\frac{1}{4} + \left(\frac{n\pi}{c}\right)^2\right]^{1/2} \tag{8}$$

($n > 0$). The first vertical mode φ_0 is always independent of height and is often called the 'barotropic mode'. For this mode, $\alpha_0 = 0$.

To examine any particular instability, say one occurring at the dimensionless vertical wavenumber $kR \equiv \hat{k}$, we choose the mean vortex radius R ($= (ab)^{1/2}$) for which $\alpha_n R = \hat{k}$, for some n, usually $n = 1$, the gravest baroclinic mode. Then, $R = \hat{k}L_R/\pi$ in the Boussinesq case and $R \simeq \hat{k}L_R/0.785$ in the compressible case (using $c = 5.86$). Note that the full height-to-width aspect ratio is only 46% greater in the compressible case than in the Boussinesq case for the same $\hat{k}$.

In all the simulations to be presented in this section, 40 vertical layers or levels are used. We originally used 20 vertical layers, and we found that the PV structures, even at fine scales, are not significantly modified upon doubling the vertical resolution. The same conclusion was reached comparing 10 and 20 layers in Dritschel & Saravanan (1994). See also Dritschel & Ambaum (1996). The initial vortex aspect ratio λ is fixed at 0.8. This is only a weak perturbation to a circular shape; more eccentric ellipses are characterized by more vigorous instabilities, the nonlinear aspects of which are qualitatively the same as for $\lambda = 0.8$. For a chosen value of the strain rate γ, the wavenumber kR is chosen to give maximum linear instability – see figure 4(*c*).

The PV is set to 4π so that the basic unit of time is a (circular) vortex rotation period. The integration time step $\Delta t = 1/40$. As for the horizontal spatial resolution, the large-scale length L is set equal to the mean vortex radius, R, and the dimensionless maximum node separation on the contours $\mu = 0.15$, corresponding to 55 points per contour at $t = 0$. The scale of surgery $\delta = \mu^2 L/4 = 0.005625R$ (Dritschel 1989).

In each simulation, the vortex is randomly disturbed initially by displacing the x- and y-coordinates of each computational node by a uniformly distributed random number between $-a$ and a, with $a = 0.01\mu R$. The vortices we are dealing with are in general very flat, so for clarity of presentation, we have chosen to draw them in a stretched vertical scale, Nz/f.

3.2. *Initially freely rotating ellipses*

For $\lambda = 0.8$, there are both long-wavelength (LW) and intermediate-wavelength (IW) instabilities, with peak growth rates at $\hat{k} \simeq 0.2720$ and 1.7075, respectively (see figure 2 or 1*c*). The IW instability is stronger if there exists a vertical mode with an appropriate wavelength, and it is seen to dominate the LW instability in simulations conducted with $kR = 0.2720$, even down to an aspect ratio of $\frac{1}{2}$. It suffices to show the IW instability growing on the gravest baroclinic mode. In a Boussinesq fluid, figure 5(*a*), the column simply tilts over then nearly recovers its initial barotropic form before repeating the process again. There is no indication that the column will break down; indeed there is no irreversible behaviour at all. This vacillation also occurs in the LW simulation, albeit on a higher baroclinic mode. In a compressible fluid, on

FIGURE 5. (*a*) Evolution of a freely rotating vortex column in a Boussinesq fluid with $\hat{k} \simeq 1.7075$ (top view). Time advances to the right and downwards; $t = t_i = 0$ in the first frame, and successive frames differ by $\Delta t_v = 20$ time units. (*b*) As in (*a*) but for a compressible fluid. Here, and in all subsequent figures, the flow is viewed from an angle of 60° from the zenith, and height is multiplied by N/f. ($t_i = 41$ and $\Delta t_v = 4$.)

(*a*)

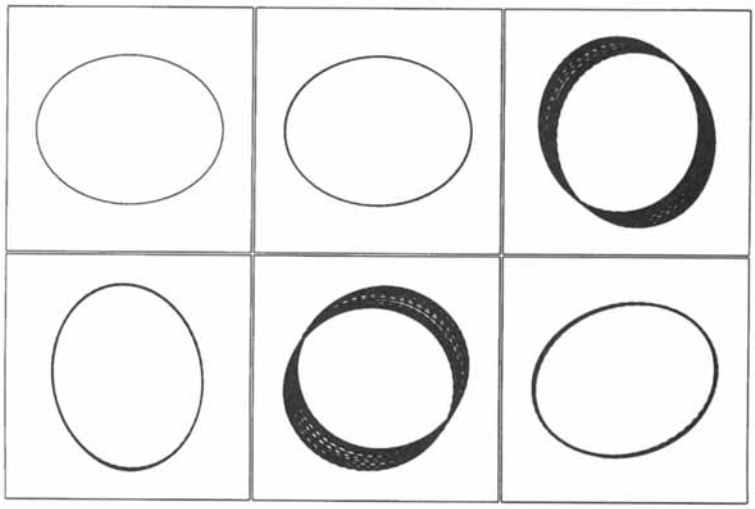

(*b*)

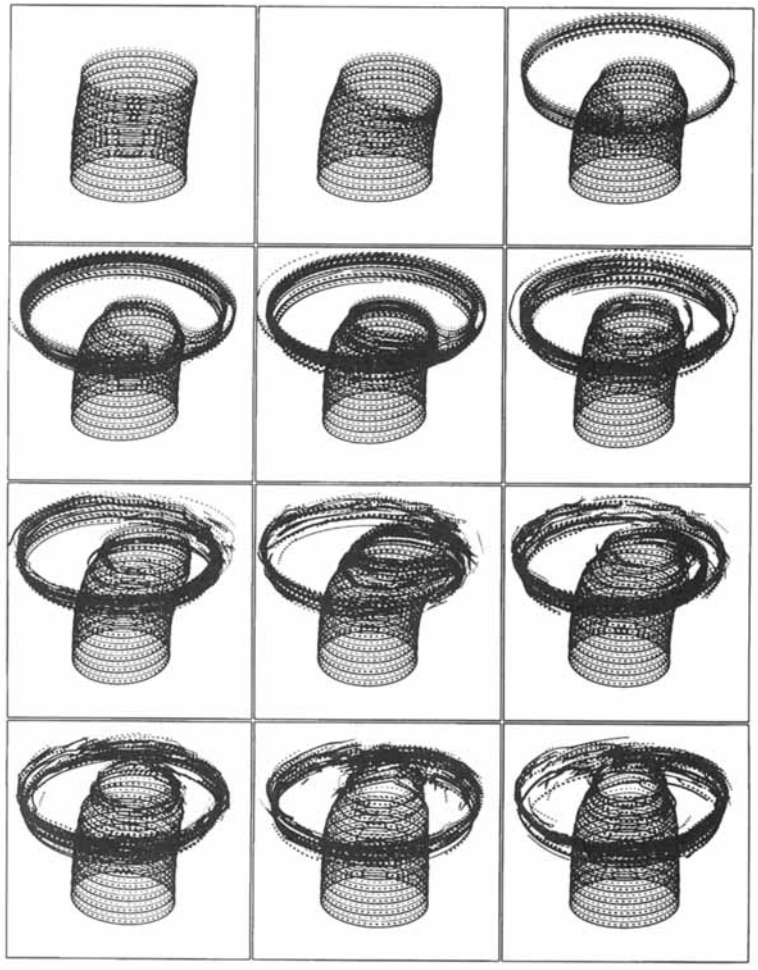

FIGURE 5. For caption see facing page.

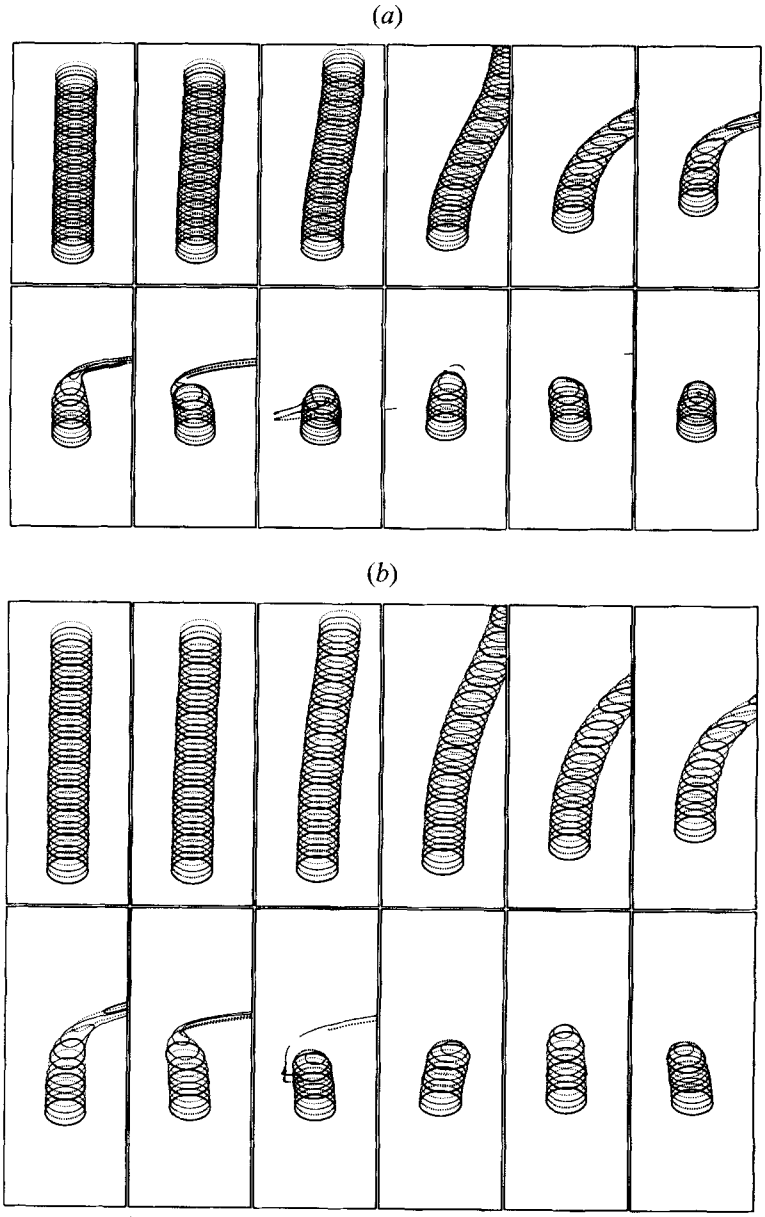

FIGURE 6. (*a*) Evolution of a strained column ($\Omega/\gamma = -1$) in a Boussinesq fluid with $\hat{k} \simeq 0.3582$. ($t_i = 20$ and $\Delta t_v = 2$.) (*b*) As in (*a*) but for a compressible fluid. ($t_i = 13$ and $\Delta t_v = 2$.)

the other hand, the upper part of the vortex is ravaged, see figure 5(*b*). This is where the density is weak and where disturbances naturally amplify most (see (8)). It takes little energy to greatly disrupt this part of the vortex. The attrition of the vortex top, to an even greater degree, also occurs in the corresponding LW simulation, owing to the greater vortex height-to-width aspect ratio.

3.3. *Initially steady, strained ellipses*

Three types of external straining flows are illustrated, having $\Omega = -\gamma$ (pure adverse shear), $-\frac{3}{2}\gamma$ and -3γ. These choices are motivated by an analysis in §4 of the typical

straining flows that occur in multiple vortex interactions. Vortex columns in straining flows with $\Omega/\gamma \geqslant -1$ (including positive values; there is progressive stabilization toward $\Omega/\gamma = 1$ and complete stability above this value; all flows with $\Omega/\gamma \geqslant 0$ are maximally unstable at $\hat{k} = 0$) have been found to evolve in a qualitatively similar way. The flow for $\Omega = -\gamma$ will serve to illustrate this. For $\lambda = 0.8$, $\gamma \simeq -0.04444$, the maximum instability occurs at $\hat{k} = \hat{k}_m = 0.3582$. Figures 6(*a*) and 6(*b*) show the evolution in a Boussinesq and in a compressible fluid, respectively, in a reference frame moving with the bottom part of the vortex column. In each case, the column is progressively tilted, until, in a Boussinesq fluid, two identical surface vortices form and move apart (the top one is not shown), or, in a compressible fluid, only one surface vortex forms in the dense fluid at the bottom. The boundaries clearly play an important role, providing greater stability than the interior. Even in a simulation designed to favour the second baroclinic mode (not shown), which in a Boussinesq fluid leads momentarily to three vortices, two at the boundaries and one in the middle, the vortex in the middle is sheared out vertically, and the surface vortices remain.

A close inspection of the bottom vortices in these two simulations reveals a height-to-mean radius aspect ratio of approximately 2.4 in the Boussinesq case and 3.3 in the compressible case. It is remarkable that these ratios are observed (within 20%) in all the simulations performed.

When $\Omega/\gamma < -1$, there is a qualitative change in the evolution. The straining flow undergoes a change in topology, as exhibited by its corresponding streamfunction,

$$\psi_{ext} = \tfrac{1}{2}\gamma[(1 - \Omega/\gamma)x^2 - (1 + \Omega/\gamma)y^2],$$

from hyperbolic to elliptic. As a result, if a column breaks apart, the background flow will not permit the pieces to drift away indefinitely.

This is illustrated for $\Omega = -\frac{3}{2}\gamma$ (and $\lambda = 0.8$) in figures 7(*a*) and 7(*b*), for a Boussinesq and a compressible fluid, respectively. In this case $\gamma \simeq -0.04077$ and $\hat{k}_m \simeq 0.4508$. In a Boussinesq fluid, the column tilts over as before, but the separation of the top and bottom parts of the column is arrested, and the vortices that form there move back toward the origin and tear apart the mass of filamentary debris in the middle as they pass each other. In a compressible fluid (figure 7*b*), a similar evolution is observed, except that only a bottom vortex remains, moving around in an elliptical orbit. The entire upper part of the vortex is rapidly shredded, though it takes longer than for the middle part.

For more extreme ratios of Ω/γ, one sees the same type of behavior as in the previous case. For example, consider $\Omega = -3\gamma$, for which $\gamma \simeq -0.03268$ and $\hat{k}_m \simeq 0.6528$. Figures 8(*a*) and 8(*b*) illustrate the flow evolution in a Boussinesq fluid and in a compressible fluid. Relative to the previous cases, the vortices that form at the domain boundaries move in more tightly confined, less eccentric orbits, clearly controlled by the external straining flow.

4. The three-dimensional instability of two interacting vortices

We now apply the results of the previous sections to the interaction of two columns of PV. Each column gives rise to a straining flow in the vicinity of the other, and, consequently, one or both of the columns may be rendered unstable.

We consider two columns of cross-sectional areas A_1 and A_2, and of PV q_1 and q_2 separated by a distance d from centre to centre. The equilibrium shapes can be calculated in detail using contour dynamics (Dritschel 1995), but here, in order to

(*a*)

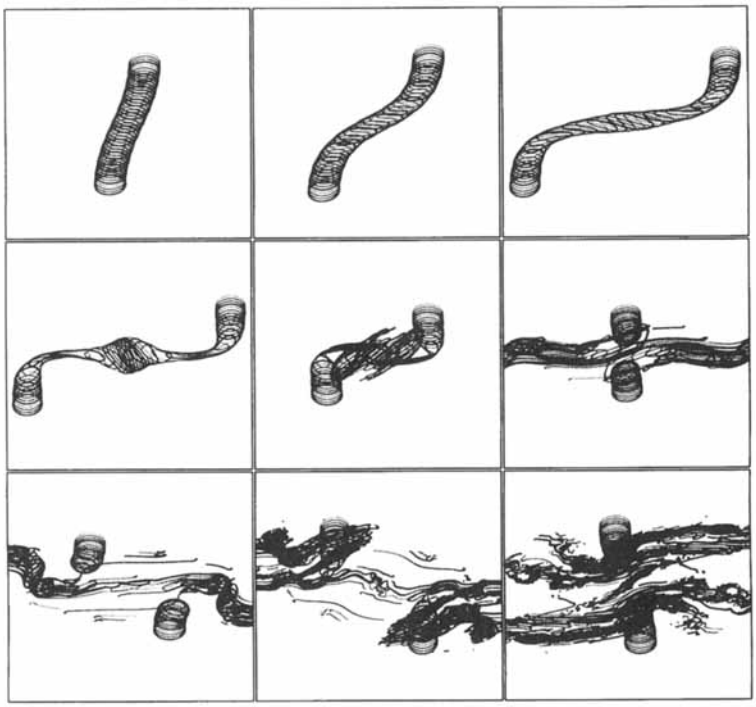

(*b*)

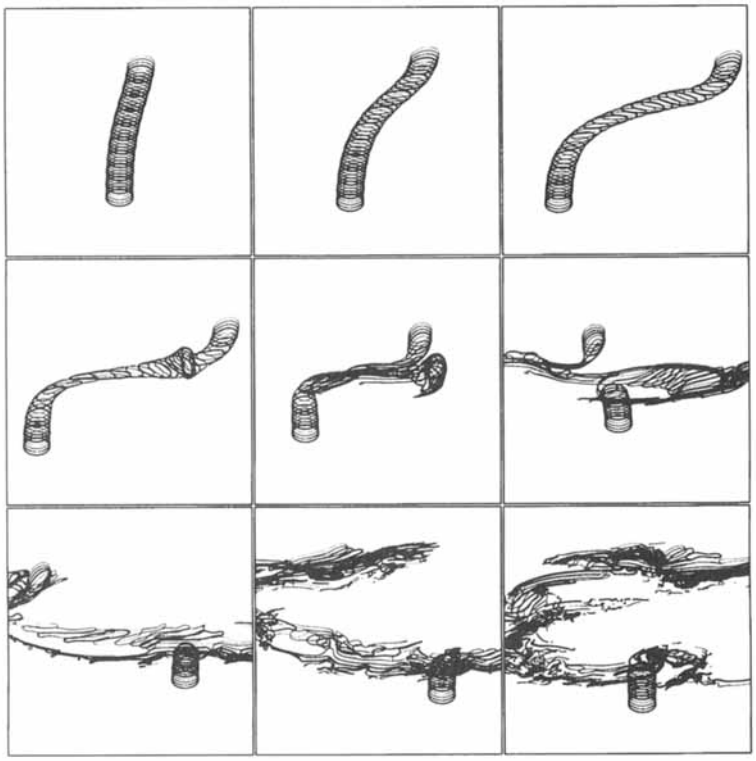

FIGURE 7. (*a*) Evolution of a strained column ($\Omega/\gamma = -\frac{3}{2}$) in a Boussinesq fluid with $\hat{k} \simeq 0.4508$. ($t_i = 26.5$ and $\Delta t_v = 2.$) (*b*) As in (*a*) but for a compressible fluid. ($t_i = 19$ and $\Delta t_v = 2.$)

(*a*)

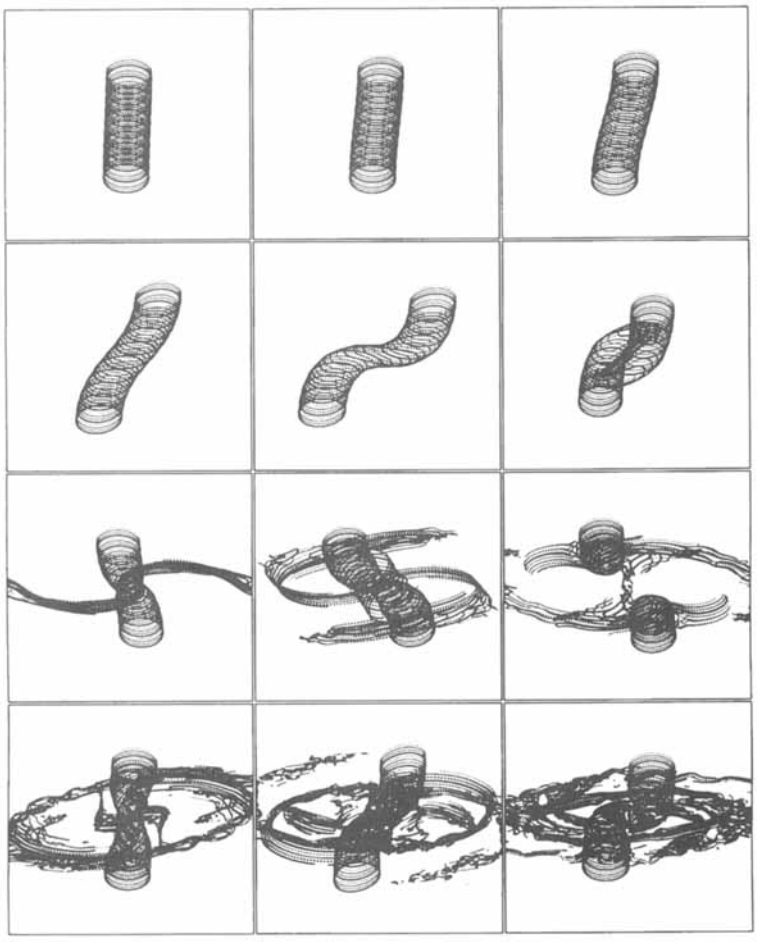

FIGURE 8(*a*). For caption see page 146.

make use of the results of previous sections, we approximate the equilibrium shapes by ellipses, using the elliptical model (Legras & Dritschel 1991) to calculate the equilibrium aspect ratios λ_1 and λ_2 (see figure 9). This is an excellent approximation for widely separated vortices, and it is this situation that most interests us here since widely-separated vortices can be unstable in a three-dimensional QG fluid while stable in a two-dimensional one.

A similar approximation is used to calculate the linear stability of the vortices: each vortex will be examined independently (but taking into account the straining flow produced by the other) rather than jointly. The validity of these approximations is checked by comparison with a full contour-dynamical treatment (i.e. using detailed boundary shapes and joint stability). This comparison gives us a deeper understanding of vortex stability.

Finally in this section, several vortex interactions are illustrated by direct numerical simulation. These permit the identification of common evolutionary sequences and give a hint at what nearly inviscid QG turbulence may be like.

(*b*)

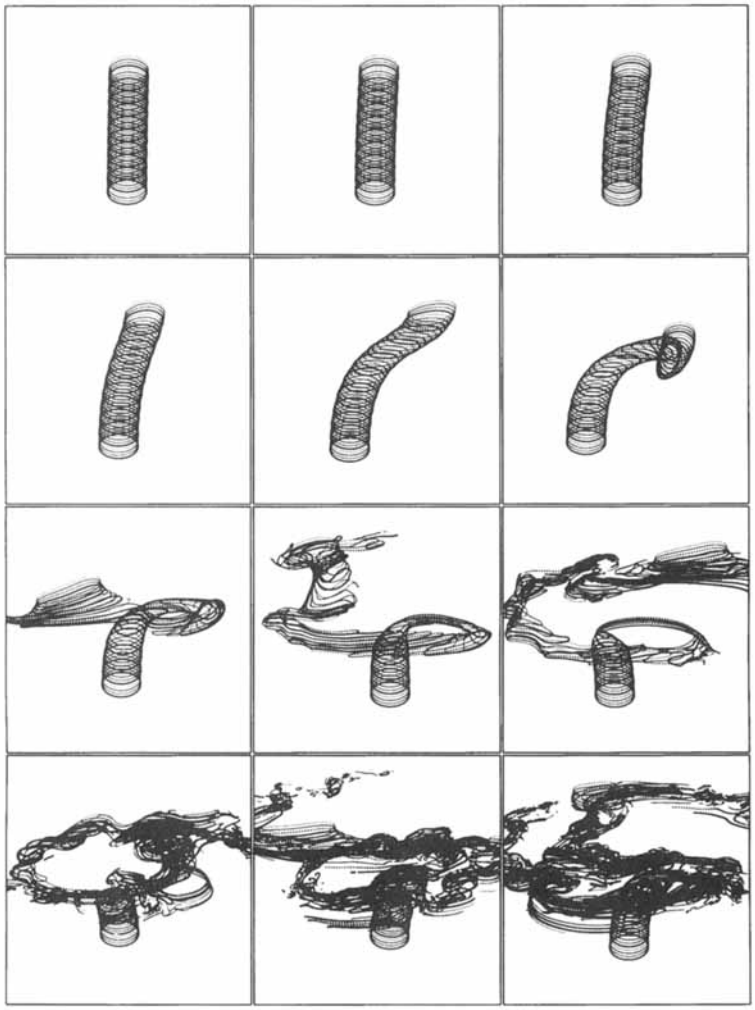

FIGURE 8. (*a*) Evolution of a strained column ($\Omega/\gamma = -3$) in a Boussinesq fluid with $\hat{k} \simeq 0.6528$. ($t_i = 24$ and $\Delta t_v = 2.$) (*b*) As in (*a*) but for a compressible fluid. ($t_i = 15.5$ and $\Delta t_v = 2.$)

4.1. *Equilibrium shapes*

The equilibria, in the form of two ellipses (figure 9), are calculated using the simplest form of the elliptical model equations. Two discrete vortices are used per vortex, $K = 2$ in Legras & Dritschel (1991). This simplest model gives results which are indistinguishable from contour dynamics as regards the onset of two-dimensional vortex merger. These equations are most conveniently expressed in the coordinates Z, the vortex centre $(X + \mathrm{i}Y)$, and $\mathscr{E}$, the vortex 'ellipticity', defined by

$$\mathscr{E} = \tfrac{1}{2}(a^2 - b^2)\mathrm{e}^{2\mathrm{i}\phi},$$

where ϕ is the orientation of the major axis with respect to the positive x-axis (see figure 10). Defining $\kappa = qA/2\pi$ and $F \equiv (a^2b^2 + |\mathscr{E}|^2)^{1/2} = \frac{1}{2}(a^2 + b^2)$, the elliptical

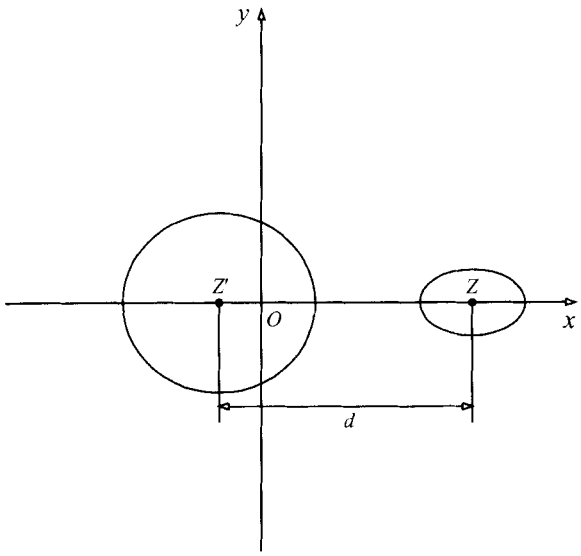

FIGURE 9. Schematic diagram of two ellipses in equilibrium.

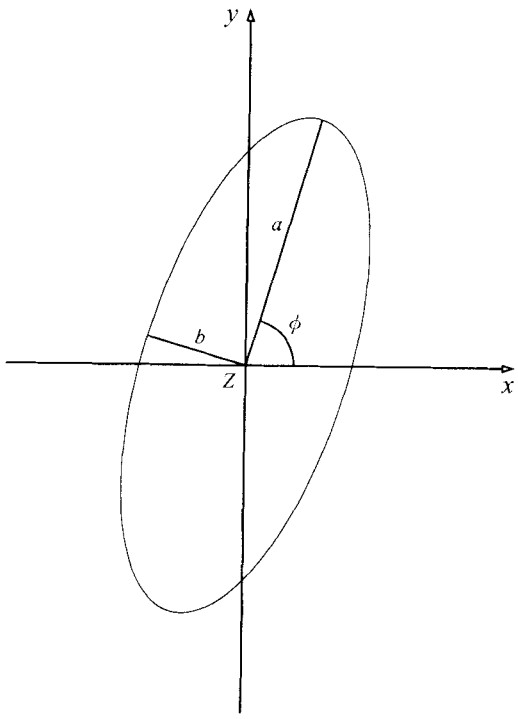

FIGURE 10. Schematic diagram for an arbitrarily oriented ellipse.

model equations for a pair of interacting vortices, $(Z, \mathscr{E})$ and $(Z', \mathscr{E}')$, are

$$\frac{\mathrm{d}Z}{\mathrm{d}t} = \alpha Z^* - \mathrm{i}\Omega Z + \kappa'[\Delta B C]^* \tag{9a}$$

$$\frac{\mathrm{d}\mathscr{E}}{\mathrm{d}t} = 2[\mathrm{i}(\kappa/(ab+F) - \Omega)\mathscr{E} + \alpha F] + 2F\kappa'[(B+\mathscr{E}')C]^* \tag{9b}$$

where

$$\Delta \equiv Z' - Z; \quad B \equiv \Delta^2 - \tfrac{1}{2}(\mathscr{E} + \mathscr{E}'); \quad C \equiv \mathrm{i}/(B^2 - \mathscr{E}\mathscr{E}') \tag{9c}$$

– the asterisk denotes complex conjugation. For generality, an external straining field is included through the terms involving $\alpha = \gamma \mathrm{e}^{2\mathrm{i}\phi_s}$, where γ is the strain rate and ϕ_s is the angle between the principal axis of strain and the positive x-axis, and a background rotation is included through the terms involving Ω.

An equilibrium is sought for two vortices lying along the x-axis ($Y = Y' = 0$) and having symmetry with respect to the x-axis ($\phi = \phi' = 0$). We require that the two vortex centres be separated by a distance d and that the centre of vorticity be at the origin (excluding the case with $\kappa + \kappa' = 0$). These two conditions determine Z and Z' (X and X') as

$$Z = \frac{\kappa' d}{\kappa + \kappa'}; \quad Z' = -\frac{\kappa d}{\kappa + \kappa'},$$

and the conditions of equilibrium ($\mathrm{d}\mathscr{E}/\mathrm{d}t = 0$ and $\mathrm{d}\mathscr{E}'/\mathrm{d}t = 0$) give two nonlinear equations for the remaining two variables $\mathscr{E}$ and $\mathscr{E}'$ (whereas both $\mathrm{d}Z/\mathrm{d}t = 0$ and $\mathrm{d}Z'/\mathrm{d}t = 0$ give a single linear equation for determining Ω in terms of the solution variables). They are efficiently solved iteratively using a guess for $\mathscr{E}$ and $\mathscr{E}'$ everywhere in (9.1b) except where these variables explicitly appear in the first term on the right-hand side. The first guess is $\mathscr{E} = \mathscr{E}' = 0$, and successive solutions are used as guesses until $\mathscr{E}$ and $\mathscr{E}'$ converge to 8 decimal places (the rate of convergence is exponential).

Once the solution is obtained, the strain produced by one vortex on the other is diagnosed by

$$\gamma = \kappa'[(B + \mathscr{E}')/(B^2 - \mathscr{E}\mathscr{E}')]^*, \tag{10}$$

which can be seen to be the correct value by comparison with the term involving a (here absent) uniform external strain α in (9.1a). The rotation rate of the strain axes, Ω, is determined as part of the iteration procedure.

We thus see that two interacting vortices can be regarded as two independent vortices in a particular rotating uniform external strain field. The results of the previous sections are thus relevant to the interaction of two vortices (indeed to the interaction of any number of vortices). Thus one immediate conclusion is that well-separated vortices, which are stable to two-dimensional disturbances, may be unstable to three-dimensional disturbances.

It is instructive to understand the nature of the rotating strain field produced by one vortex in the vicinity the other. To a first approximation (see (10)), $\gamma = -s\kappa'/\Delta^2$ and $\gamma' = -s\kappa/\Delta^2$, where the factor s, equal to $+1$ for like-signed vortices and -1 for opposite-signed ones, arises from the orientation of the vortices (like-signed vortices have semi-major axes lying along the line passing through the vortex centres, while opposite-signed vortices have them lying perpendicular to it). Likewise, $\Omega = (\kappa+\kappa')/\Delta^2$. In the previous sections, these rate quantities were made dimensionless on the PV value in the vortex, here q or q'. Thus, the dimensionless strain and background rotation rates for the unprimed vortex would be $-s\kappa'/q\Delta^2$ and $(\kappa+\kappa')/q\Delta^2$. Likewise, those for the primed vortex would be $-s\kappa/q'\Delta^2$ and $(\kappa+\kappa')/q'\Delta^2$. These dimensionless

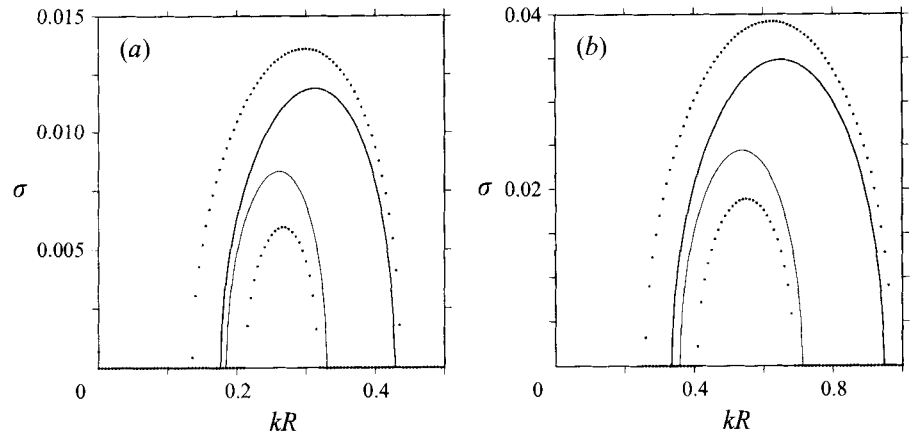

FIGURE 11. Comparison between the growth rates obtained using the elliptical model (solid lines) and those obtained using a full contour-dynamical treatment (dotted lines) for two equal-PV vortices having an area ratio of 0.7. (*a*) $d = 5R$, (*b*) $d = 3R$.

quantities were referred to as γ and Ω in the previous sections, and we return to those meanings presently.

For two identical vortices, $\kappa = \kappa'$, we see that $\Omega = -2\gamma$, while for two opposite vortices, $\kappa = -\kappa'$, we have $\Omega = 0$. For $\kappa = \frac{1}{2}\kappa'$, we have $\Omega = -3\gamma$ for the smaller vortex and $\Omega = -\frac{3}{2}\gamma$ for the larger, while for $\kappa = -\frac{1}{2}\kappa'$, we have $\Omega = +\frac{1}{2}\gamma$ for the smaller vortex and $\Omega = -\gamma$ for the larger. In no case can Ω/γ exceed 1. $\Omega/\gamma = 1$ corresponds to a pure cooperative shear. From these results, we can give a physical interpretation to the straining flows considered in the previous section.

4.2. *Linear stability*

The approximate linear stability of the system of two columnar vortices, of equal and of opposite-signed PV, can be inferred from the results of §2, i.e. from the stability of each vortex in the fixed strain field of the other. The results in a particular case are compared to a full contour-dynamical treatment of the problem, using equilibrium vortex shapes calculated by contour dynamics (Dritschel 1995) and joint stability, computed as described in §2.1.

First, let us examine the comparison between the approximate and full treatment of the problem. For two like-signed vortices of cross-sectional area ratio 0.7 and total area πR^2, the growth rate versus $\hat{k} = kR$, for $d = 5R$ and $d = 3R$, is shown in figures 11(*a*) and 11(*b*), respectively, with dotted lines for the full results and solid lines for the approximate results. Though there is a clear discrepancy, the results for a single vortex in strain do give at least a qualitative guide to the joint stability of the vortices. The maximum growth rates differ by about 10% for the upper curves and between 20% and 30% for the lower curves.

The discrepancy is due to the neglected coupling between the disturbances on the two vortices in the single-vortex stability analysis. Since the vortices are not greatly different from a circular shape, the approximate coupling between the vortices, for a mode with azimuthal wavenumber m, would be expected to scale with $K_m(kd)$, where K_m is the mth-order modified Bessel function. For small argument, $K_m \sim (R/d)^m$, which is the two-dimensional coupling strength. However, we see in the figures that $kd = (kR)(d/R) = \hat{k}(d/R) \gtrsim 1$, and for $kd \gg 1$, $K_m \sim (kd)^{-1/2}\exp(-kd)$, so that the coupling becomes exponentially weak with increasing kd. Looking at figures 11(*a*) and

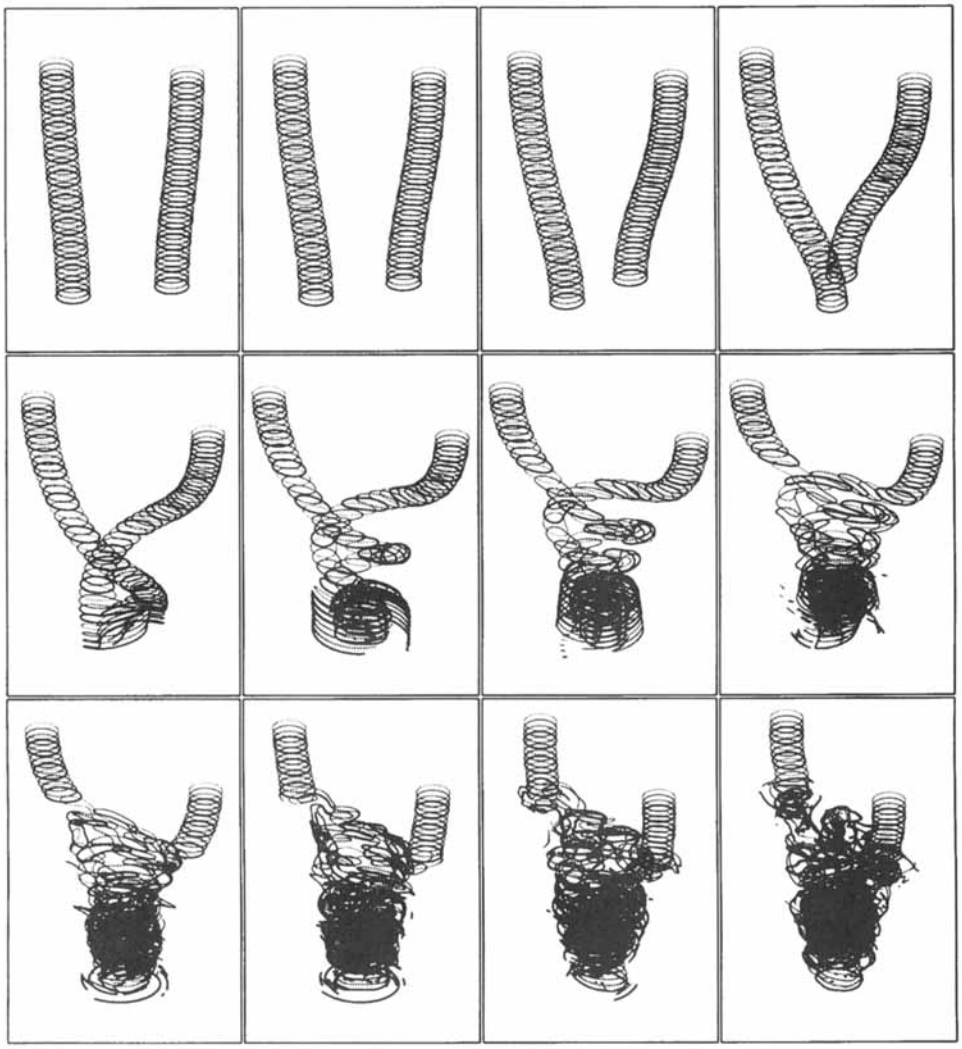

FIGURE 12. The evolution of two identical vortex columns, each of cross-sectional area $\frac{1}{2}\pi R^2$, separated by $d = 5R$ initially, and with R chosen so that $\hat{k} = 0.2\sqrt{2}$. ($t_i = 37.5$ and $\Delta t_v = 2$.)

11(*b*), it may be noticed that the two sets of results for $d = 5R$ do not compare any better than those for $d = 3R$, contrary to what might be expected. The explanation is that kd is similar in the two cases, so the mode-coupling strength is similar. The discrepancy is not a function of d/R alone.

The conclusion is that we can approximately describe the instability of a two-column system in terms of the instability of a single column in strain. Contour plots of growth rate as a function of kR and d/R can be shown, but do not reveal any surprises: the larger vortex is always less unstable because it is less deformed (λ is closer to unity). The growth rates of disturbances on the smaller vortex always exceed, up to several times, the growth rates of disturbances on the larger vortex. The true difference is actually greater than the single-column problem indicates – refer back to figure 11 for the comparison with the two-column problem. For like-signed vortices, the peak growth rates for the smaller vortex occur at higher kR than for the larger

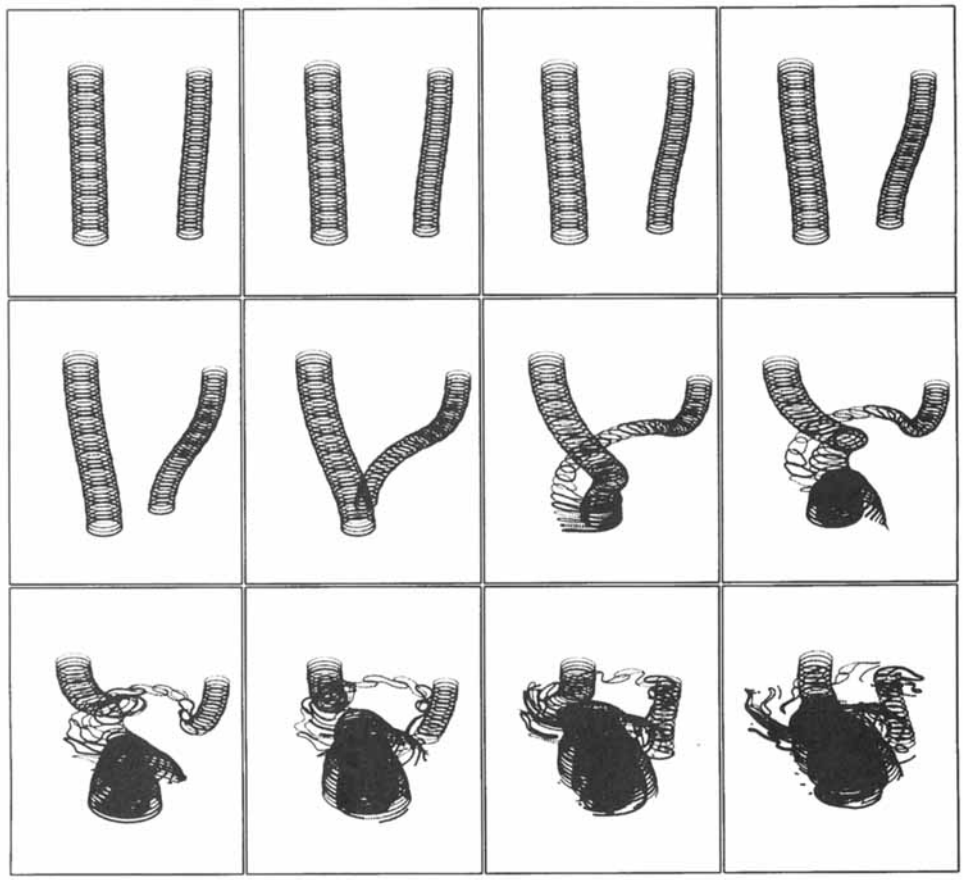

FIGURE 13. The evolution of two equal-PV vortex columns of area ratio $\alpha = \frac{1}{2}$, total area πR^2, and separated by $d = 5R$ initially, with $\hat{k} = 0.2\sqrt{3}$. ($t_i = 45$ and $\Delta t_v = 2$.)

vortex. For opposite-signed vortices, the peak growth rates for the smaller vortex always occur at $k = 0$; however, the range of unstable wavenumbers extends beyond the corresponding range for the larger vortex.

4.3. *Nonlinear evolution*

We next examine several examples of the interaction of two vortex columns, initially in approximate equilibrium, in a Boussinesq fluid. In the first series of simulations, the two columns have the same PV, have a combined area of πR^2, and are separated by a distance $d = 5R$ from centre to centre. The value of $\hat{k}$ is chosen so that the smaller vortex is maximally unstable; if R_2 is the smaller vortex radius, this occurs very near to $kR_2 = 0.2$ or $\hat{k} = 0.2R/R_2 = 0.2[(1+\alpha)/\alpha]^{1/2}$, where α is the vortex area ratio.

Figure 12 shows the evolution of two identical columns, $\alpha = 1$, in a rotating frame of reference in which undisturbed columns would remain stationary. Each vortex initially experiences a straining flow having $\Omega = -2\gamma$. The two columns tilt, as in the previous single-column simulations, bringing the columns closer together at the bottom, where they rotate faster, leading to a double-helix structure. The parts at the bottom collide, merging into a coherent compound vortex of a semi-ellipsoidal shape

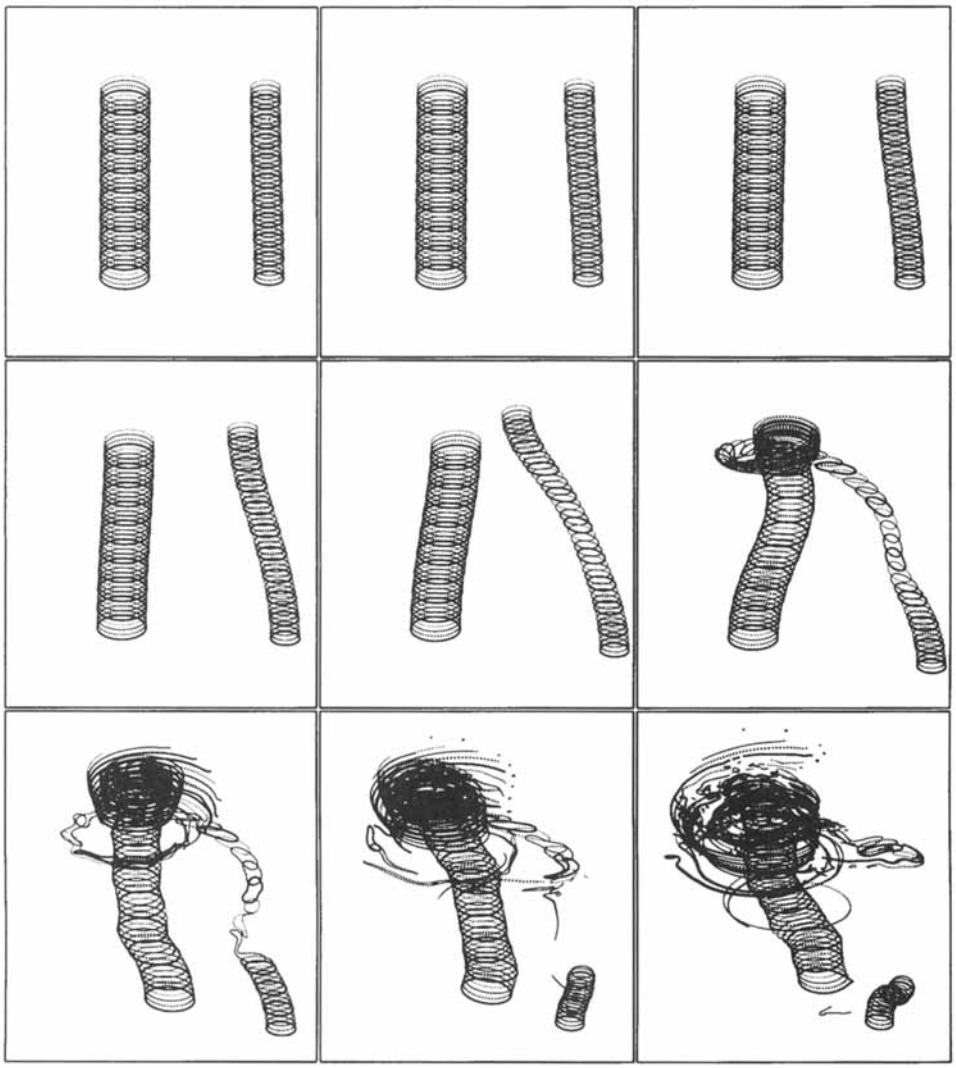

FIGURE 14. As in figure 13, except $\alpha = \frac{1}{3}$ and $\hat{k} = 0.4$. ($t_i = 35.5$ and $\Delta t_v = 4$.)

within a blanket of encircling filamentary debris. Two baroclinic vortices also remain at the upper surface, and the PV in the middle becomes progressively shredded and disorganized. In a compressible fluid (not shown), only a bottom vortex forms.

Figure 13 shows the evolution for area ratio $\alpha = \frac{1}{2}$. The initial straining field has the form $\Omega = -\frac{3}{2}\gamma$ in the vicinity of the larger vortex (cf. figure 7*a*), and $\Omega = -3\gamma$ in the vicinity of the smaller (cf. figure 8*a*). The initial evolution again displays a tilting of the columns, though here the smaller column tilts to a greater degree. The columns wind around each other, and the bottom parts merge together into a single compound vortex, as in the previous simulation. In this simulation, the semi-ellipsoidal form of the bottom vortex is more evident, though it is masked by a sloping dome of filaments. Again, two robust baroclinic vortices form at the upper surface, and the PV in the middle gets shredded.

Upon further decreasing the area ratio, a qualitative change takes place – see figure 14 for $\alpha = \frac{1}{3}$. (Initially, $\Omega = -\frac{4}{3}\gamma$ is experienced by the larger vortex and $\Omega = -4\gamma$ is

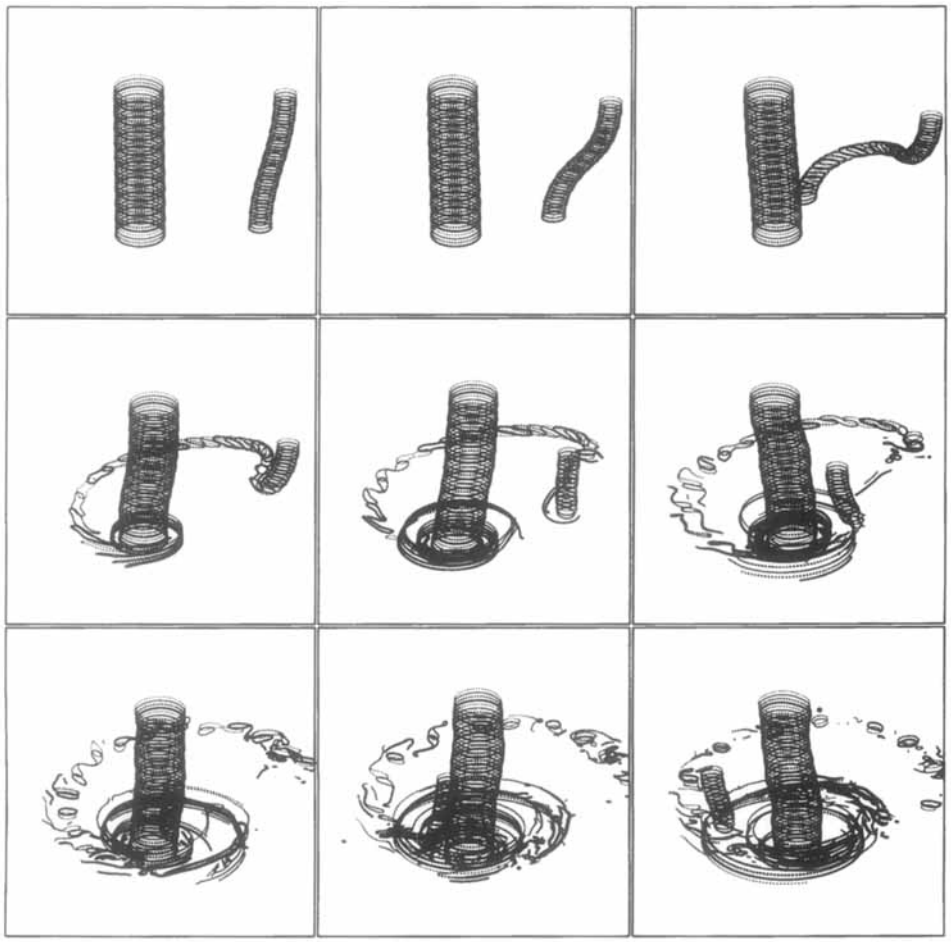

FIGURE 15. As in figure 13, except $\alpha = \frac{1}{5}$ and $\hat{k} = 0.2\sqrt{6}$. ($t_i = 47$ and $\Delta t_v = 4$.)

experienced by the smaller.) First of all, the two columns approach at the top instead of the bottom. In fact, in a Boussinesq fluid, either surface is equally favoured; another disturbance might have caused the vortices to approach at the bottom. The more significant change is the nature of the collision: the larger vortex column does not break up, though it is severely deformed (note the presence of short vertical waves). The upper part of the smaller vortex is completely strained out, and there is an insignificant change in the cross-sectional area of the larger vortex. Part of the smaller vortex remains at the lower surface, which appears about to shorten further.

As a final case, figure 15 shows the evolution for an even smaller area ratio, $\alpha = \frac{1}{5}$. (Initially, $\Omega = -\frac{6}{5}\gamma$ is experienced by the larger vortex and $\Omega = -6\gamma$ is experienced by the smaller.) The columns now revert back to colliding at the bottom. This simulation is similar to the previous one, though here the larger column is much more weakly disturbed, and the complete straining out of the smaller is more clearly seen.

It is remarkable that these three-dimensional interactions exhibit the same five regimes of interactions observed in two-dimensional (Dritschel & Waugh 1992), often in combination (at different heights). In figure 15, we have *elastic interaction* at the top, *partial straining out* below that, and *complete straining out* all the way to the

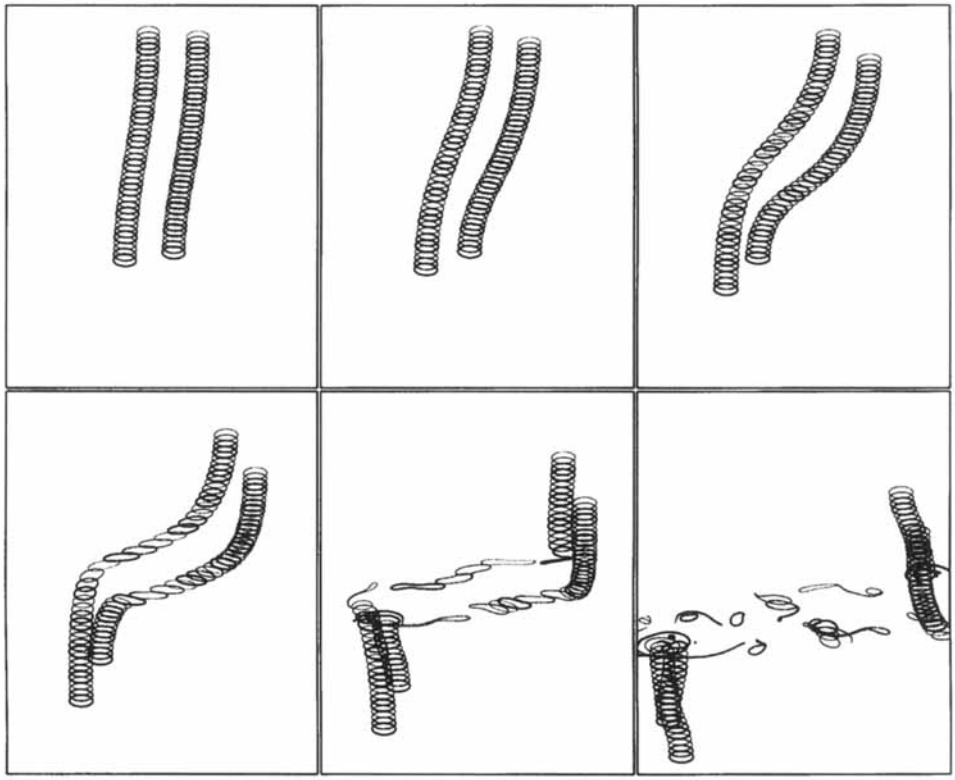

FIGURE 16. The evolution of two equal-area, opposite-PV vortex columns, each of cross-sectional area $\frac{1}{2}\pi R^2$, separated by $d = 3R$ initially, and $\hat{k} = 0.2$. ($t_i = 43$ and $\Delta t_v = 4$.)

bottom (figure 14 is just the reverse). In figures 12 and 13, we have in addition *partial merger* and *complete merger* near the bottom of the domain, i.e. all five regimes in one calculation!

To change tack, consider the interaction of two columns of opposite PV. As above, we take the total area of the columns to be πR^2 and separate them by a distance $d = 3R$ from centre to centre. The vortices are closer than in the like-signed interactions above to give comparable instability wavelengths. Figure 16 shows the evolution of two equal-sized columns, $\alpha = 1$ (corresponding to $\Omega = 0$), with R chosen so that $\hat{k} = 0.2$. The columns tilt and form vortices at the top and bottom boundaries, as occurs in single-vortex simulations having $\Omega = 0$ (not shown), which subsequently pair and travel apart in a direction perpendicular to the original direction followed by the two columns.

Figure 17 shows the evolution for an area ratio $\alpha = \frac{1}{2}$ with $\hat{k} = \frac{1}{10}\pi$. (Initially, $\Omega = -\gamma$ is experienced by the larger vortex and $\Omega = \frac{1}{2}\gamma$ is experienced by the smaller.) Though the smaller column is more greatly deformed early on, both columns split vertically, and the four resulting baroclinic vortices, mismatched in each part of the domain, move about in a complicated pattern. There is remarkably little filamentary debris generated in these opposite-signed vortex interactions, and the vortices attached to the surfaces are significantly taller than their counterparts in the like-signed interactions (figures 12 to 15). The vortices here are also much more circular (due to the strength and the nature of the straining flow) which accounts for their greater vertical extent.

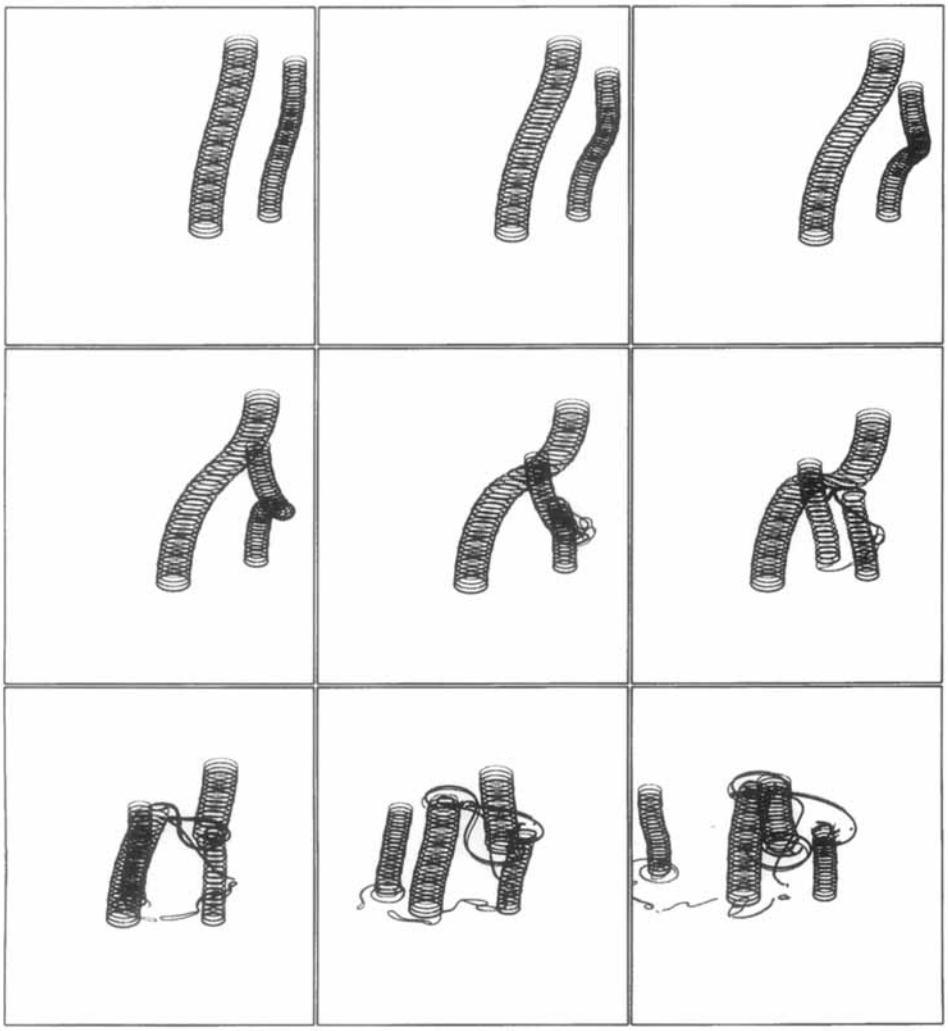

FIGURE 17. As in figure 16, but for area ratio $\alpha = \frac{1}{2}$ and $\hat{k} = \frac{1}{10}\pi$. ($t_i = 45.5$ and $\Delta t_v = 2$.)

Just above the area ratio $\alpha = \frac{1}{4}$, the vortex interaction changes character — see figure 18 for $\alpha = \frac{1}{4}$ when $\hat{k} = 0.34$. (Initially, $\Omega = -3\gamma$ is experienced by the larger vortex and $\Omega = \frac{3}{4}\gamma$ is experienced by the smaller.) Now, only the smaller column breaks apart. The larger vortex remains intact despite a substantial tilt. At $\alpha = 0.3$ (not shown), the larger vortex breaks apart, as in figure 17.

5. Discussion

This paper has examined the three-dimensional stability of both freely rotating and strained elliptical columns of uniform potential vorticity in a quasi-geostrophic fluid. The freely-rotating case was examined previously by Miyazaki & Hanazaki (1994), who determined the linear stability characteristics. Here, we have also examined the nonlinear evolution, using a high-resolution contour surgery code (Dritschel &

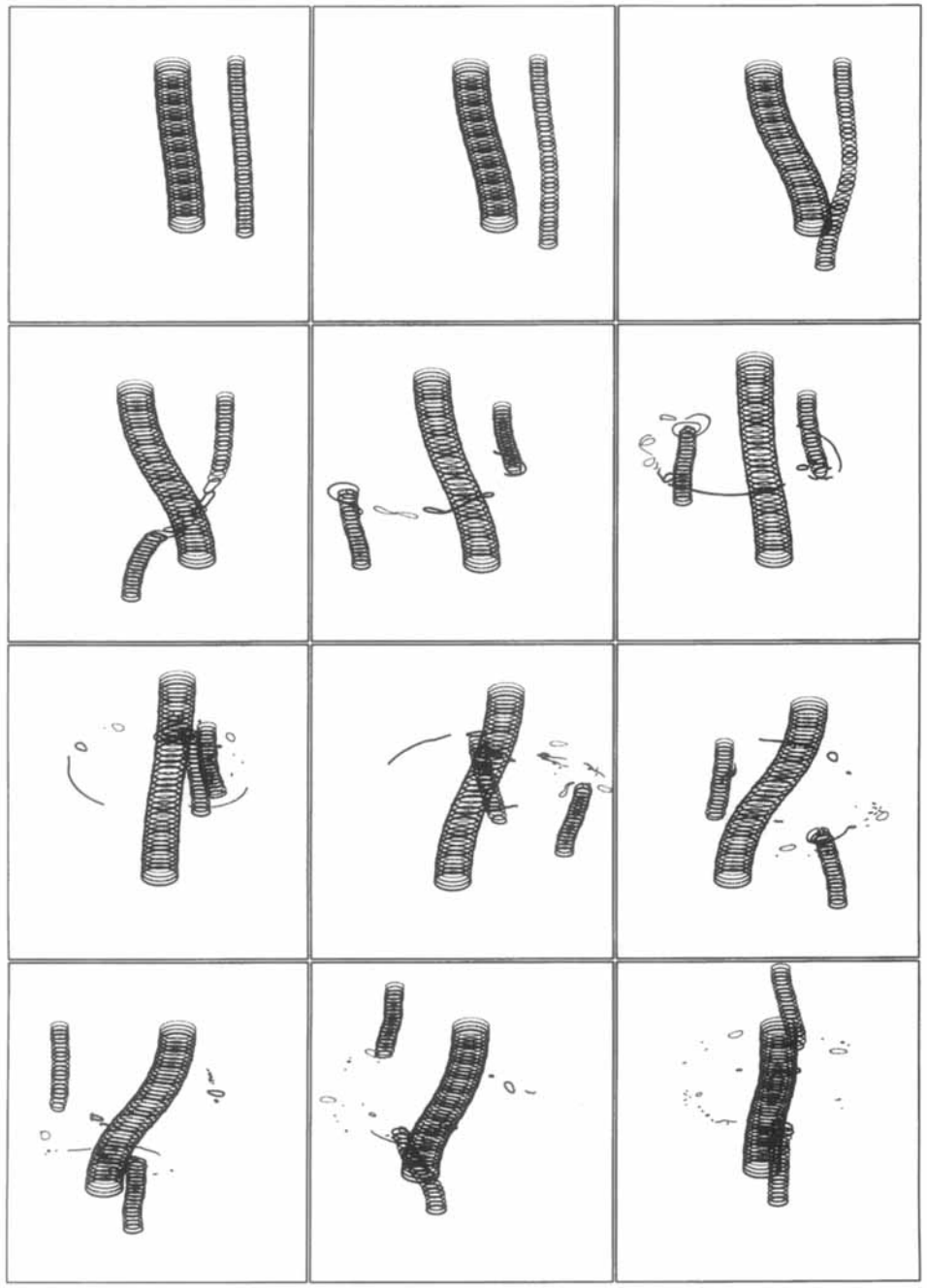

FIGURE 18. As in figure 16, but for area ratio $\alpha = \frac{1}{4}$ and $\hat{k} = 0.34$. ($t_i = 44$ and $\Delta t_v = 4$.)

Saravanan 1994), in both a Boussinesq and a compressible fluid having constant buoyancy frequency.

In the absence of strain, three-dimensional instability may occur for tall vortices arbitrarily close to a circular form (when such vortices are stable to two-dimensional disturbances). However, this instability does not break up the vortex column, but rather leads to vacillation and a limited amount of filamentation. Even in a compress-

ible fluid, where the upper part of the vortex is ravaged, a core of coherent vorticity persists.

In the presense of strain, however, this three-dimensional instability causes a breakdown of the vortex column. A common evolutionary sequence has been identified: a tilting of the vortex column followed by the formation of a baroclinic vortex dome at the bottom and, for a Boussinesq fluid, a symmetrical vortex dome at the top. In a compressible fluid, a vortex dome cannot form in the low-density part of the domain due to the stronger effect of the straining flow there.

The results for strain were shown to be related to the interaction between two vortex columns. Nonlinear simulations were performed for a Boussinesq fluid. Like-signed columns were shown to tilt initially, consistent with the results found for uniform external straining, and then strongly interact with each other at one of the surfaces, resulting in a single wider baroclinic vortex there for area ratios exceeding one third. For smaller area ratios, much of the smaller column is twisted about and dispersed around the larger column, leaving the latter intact. Part of the smaller vortex survives at one of the boundaries and orbits the larger vortex.

For opposite-signed columns, the lower and upper parts split apart and pair with their neighbours, again resulting in baroclinic vortex domes attached to the domain boundaries, for area ratios exceeding one quarter. For smaller area ratios, the larger vortex remains unsplit. The vortices are generally taller than those found in like-signed interactions due to their more circular shape, and this is a consequence of the weaker strength and less-obtrusive nature of the straining field felt in opposite-signed interactions.

A principal conclusion is that, if a vortex column is experiencing two-dimensional strain, which is inevitable in either a multi-vortex environment or e.g. in the presence of topographic forcing, and if the column is narrow enough (of height-to-width aspect ratio exceeding about $3f/N$), then the vortex column will break down into one or two baroclinic boundary vortices (which may subsequently merge with other boundary vortices).

Is this observed? Hua & Haidvogel (1986) reported the development of baroclinic vortices of comparable height-to-width aspect ratios in simulations of Boussinesq QG turbulence maintained by baroclinic instability (by surface temperature gradients at the upper and lower surfaces). In higher-resolution simulations of unforced (freely decaying) Boussinesq QG turbulence, McWilliams (1989, 1990) showed that baroclinic vortices are much more likely to be found at the top and bottom boundaries than in the middle. His data analysis furthermore revealed that the average height-to-width aspect ratio of such vortices is approximately $1.7f/N$ (this is comparable to the value of $2.4f/N$ found here for the vortex domes emerging from the columnar instability). McWilliams (1990) attributed the breakdown of tall columns to vertical shear. The present study has shown that horizontal shear is sufficient.

More recently, McWilliams, Weiss & Yavneh (1994) have suggested that the process of vortex 'alignment' (Polvani 1991; Viera 1995) will result in approximately columnar vortices at long times (as suggested by Rhines 1979 but not observed by Hua & Haidvogel 1986 nor by McWilliams 1989). The present study, for a nearly-dissipationless fluid, favours rather the original picture of vortex domes attached to the domain boundaries with persistently disorganized, thinning filamentary debris between (this has recently been confirmed in the work of Dritschel & Ambaum 1996). We suggest that the accumulative effect of horizontal dissipation, which is not insignificant in McWilliams *et al.* simulation, biases the flow to become more barotropic. As the vortices spread horizontally, they can more easily align vertically

and thereby grow in height. Would the same be observed at much lower levels of dissipation, when vortex collisions may result in little if any horizontal spreading, judging from nearly dissipationless simulations of two-dimensional turbulence (Dritschel 1993, 1995)?

Elements of this instability are also evident in the two-layer simulations of Polvani (1991). He studied the alignment of two vortex patches, one in each layer, of identical PV and initially circular, by placing the centres of the patches a certain distance apart and performing contour dynamical simulations of the evolution. He found that alignment does not occur in the 'weakly coupled' limit, when the radius of deformation is larger than the initial vortex radius. The inverse radius of deformation in that study is identical to k in the present one, showing that $kR < 1$ results in no alignment. He argues that the existence of a nearby (in parameter space) linearly stable, circular column prevents alignment, but the present study suggests rather that it is due to the existence of a nearby linearly unstable, elliptical column. In fact, we conducted a two-layer simulation of an initially elliptical column, and it does exhibit de-alignment, then re-alignment, and so on nearly periodically.

More recently, Viera (1995) studied the alignment of a tilted three-dimensional column of uniform PV, of finite vertical extent, in a horizontally *and* vertically unbounded Boussinesq QG fluid. The tallest vortex he considered had a height-to-width aspect ratio of f/N, and this vortex exhibited rapid initial alignment (at early times; a longer simulation appears to be required). This height-to-width aspect ratio is the minimum required for the instability of a freely rotating elliptical column *between rigid surfaces*, which we have seen exhibits vacillation, like in the two-layer simulation mentioned previously. It is difficult to draw further conclusions, since Viera (1995) considered a vertically unbounded fluid.

In real, naturally occurring flows, the development of this columnar instability would be difficult to observe, since it would likely take place simultaneously with vortex formation, such as the spinning off of a smaller vortex from a larger, and would thus not be interpreted as an instability. However, the height-to-width aspect ratios of typical atmospheric and oceanic vortices do satisfy the constraint that they be less than about $3f/N$. For example, the stratospheric polar vortex is normally about 6 scale heights tall and 3 Rossby radii wide, giving it an aspect ratio of about $2f/N$. The surface vortices spun off the Gulf Stream and the Kuroshio Current also fit the pattern. Remarkably, even tropical cyclones in their decay stage (when the convection has largely halted) – which are not QG vortices – have a height-to-width aspect ratio of about $3f/N$ (meaning 3 scale heights tall and 1 deformation radius wide; see Shapiro & Franklin 1994). Finally, primitive-equation simulations of vortex merger by Wang & Holland (1995) exhibit remarkably similar patterns of behavior to those seen in the present QG simulations. It might not be a coincidence, and it motivates a closer examination of the stability of tall vortex columns in general.

A number of research questions are raised. How does this instability limit the height of vortices over topography (fixed as in the ocean, variable as at the base of the stratosphere)? A previous study using QG dynamics to study the effect of topographic forcing on the polar vortex (Dritschel & Saravanan 1994) concluded that the forcing is predominantly two-dimensional in character, at least if the horizontal scale of the forcing is comparable to the scale of the vortex. Hence, one should see the columnar instability, manifested in the destruction of the upper part of the vortex, if the domain height is extended. This has been confirmed (D. W. Waugh, personal communication), and a quantitative study is underway.

Another question is the effect of using a free upper surface rather than a rigid lid.

In this case, the boundary condition there gets modified to

$$\partial\psi/\partial z + B(\psi/H) = 0$$

where $B = f^2 L_R^2/gH$, and g is the gravitational acceleration. For $B \ll 1$, the surface again looks rigid. In fact, $B \ll 1$ for typical ocean vortices having a horizontal scale of L_R. For much larger vortices, such as vortices in the atmospheres of other planets, it is possible to have $B \approx 1$. Exactly what happens at the upper surface as a result of a columnar vortex instability needs to be examined. The basic state used in this paper is no longer appropriate, since there is no two-dimensional (vertically independent) mode for $B > 0$. One can still find a basic state $(\psi_e(x, y)\phi_1(z), q_e(x, y)\phi_2(z))$ consisting of a vortex column of uniform q_e in an external straining flow, only it must satisfy $\nabla_h^2\psi_e - \alpha_1^2\psi_e = q_e$, where $\alpha_1 > 0$ is the inverse deformation radius for the gravest vertical mode ϕ_1. Such solutions have been calculated by Polvani, Flierl & Zabusky (1989).

The apparently greater robustness of baroclinic boundary vortices compared to those in the interior is another topic which deserves study. By subjecting initially circular vortices of various height-to-width aspect ratios to a slowly growing shear, we expect to find that the vortex will destabilize at some critical shear by shedding its vertical extremity(ies), and thereby become stouter. We expect to determine a relationship between the critical shear and the vortex height-to-width aspect ratio, for both boundary and interior vortices.

The effect of a planetary vorticity gradient (variable f) also merits study. The basic state used here is no longer steady, and the initial (barotropic) evolution starting, say, from a circular column, would involve the wrapping around of planetary vorticity contours followed by an elliptical deformation (see e.g. Sutyrin *et al.* 1994). As the latter gives rise to horizontal straining and horizontal straining is a crucial ingredient of the tall-column instability, a tall column in a planetary vorticity gradient may also break down into baroclinic surface vortices. This is at present under investigation.

There are also questions about the effect of *vertical* environmental shear (e.g. a uniform flow increasing with height), varying PV up the vortex column (which is thought to occur in the polar stratospheric vortex), and non-uniform horizontal distributions of PV (e.g. a Gaussian core). Work is underway to explore these questions.

D.G.D. is supported by the UK Natural Environmental Research Council. Both authors received additional support from the Isaac Newton trust, NATO, the European Community (CHRX-CT92-0001), and EPSRC (for computing time).

REFERENCES

BAYLY, B. J., HOLM, D. D. & LIFSCHITZ, A. 1995 Three-dimensional stability of elliptical vortex columns in external strain flows. *Phil. Trans. R. Soc. Lond.* A **354**, 895–926.

DRITSCHEL, D. G. 1986 The nonlinear evolution of rotating configurations of uniform vorticity. *J. Fluid Mech.* **172**, 157–182.

DRITSCHEL, D. G. 1988 Nonlinear stability bounds for inviscid, two-dimensional parallel or circular flows with monotonic vorticity, and the analogous three-dimensional quasi-geostrophic flows. *J. Fluid Mech.* **191**, 511–547.

DRITSCHEL, D. G. 1989 Contour dynamics and contour surgery: numerical algorithms for extended, high-resolution modelling of vortex dynamics in two-dimensional, inviscid, incompressible flows. *Comput. Phys. Rep.* **10**, 77–146.

DRITSCHEL, D. G. 1990 The stability of elliptical vortices in an external straining flow. *J. Fluid Mech.* **210**, 223–261.

DRITSCHEL, D. G. 1993 Vortex properties of two-dimensional turbulence. *Phys. Fluids* A **5**, 984–997.

DRITSCHEL, D. G. 1995 A general theory for two-dimensional vortex interactions. *J. Fluid Mech.* **293**, 269–303.

DRITSCHEL, D. G. & AMBAUM, M. H. P. 1996 A contour-advective semi-Lagrangian numerical algorithm for simulating fine-scale conservative dynamical fields. *Q. J. R. Met. Soc.* (in press).

DRITSCHEL, D. G. & SARAVANAN, R. 1994 Three-dimensional quasi-geostrophic contour dynamics, with an application to stratospheric vortex dynamics. *Q. J. R. Met. Soc.* **120**, 1267–1297.

DRITSCHEL, D. G. & WAUGH, D. W. 1992 Quantification of the inelastic interaction of two asymmetric vortices in two-dimensional vortex dynamics. *Phys. Fluids* A **4**, 1737–1744.

HOSKINS, B. J., MCINTYRE, M. E. & ROBERTSON, A. W. 1985 On the use and significance of isentropic potential-vorticity maps. *Q. J. R. Met. Soc.* **111**, 877–946.

HOUGHTON, J. T. 1986 *The Physics of Atmospheres*, 2nd Edn. Cambridge University Press.

HUA B. L. & HAIDVOGEL, D. B. 1986 Numerical simulations of the vertical structure of quasi-geostrophic turbulence. *J. Atmos. Sci.* **43**, 2923–2936.

KIDA, S. 1981 Motion of an elliptical vortex in a uniform shear flow. *J. Phys. Soc. Japan* **50**, 3517–3520.

KIRCHHOFF, G. 1876 In *Vorlesungen über mathematische Physik*. Leipzig: Mechanik.

LEGRAS, B. & DRITSCHEL, D. G. 1991 The elliptical model of two-dimensional vortex dynamics. Part I: the basic state. *Phys. Fluids* A **3**, 845–854.

LEGRAS, B. & DRITSCHEL, D. G. 1993 Vortex stripping and the generation of high vorticity gradients in two-dimensional flows. *Appl. Sci. Res.* **51**, 445–455.

LOVE, A. E. H. 1893 On the stability of certain vortex motions. *Proc. Lond. Math. Soc.* **35**, 18.

MARIOTTI, A., LEGRAS, B. & DRITSCHEL, D. G. 1994 Vortex stripping and the erosion of coherent structures in two-dimensional flows. *Phys. Fluids* **6**, 3954–3962.

MCINTYRE, M. E. 1995 The stratospheric polar vortex and sub-vortex: fluid dynamics and midlatitude ozone loss. *Phil. Trans. R. Soc. Lond.* **352**, 227–240.

MCWILLIAMS, J. C. 1989 Statistical properties of decaying geostrophic turbulence. *J. Fluid Mech.* **198**, 199–230.

MCWILLIAMS, J. C. 1990 The vortices of geostrophic turbulence. *J. Fluid Mech.* **219**, 387–404.

MCWILLIAMS, J. C., WEISS, J. B. & YAVNEH, I. 1994 Anisotropy and coherent vortex structures in planetary turbulence. *Science* **264**, 410–413.

MEACHAM, S. P. 1992 Quasi-geostrophic, ellipsoidal vortices in a stratified fluid. *Dyn. Atmos. Oceans* **16**, 189–223.

MELANDER, M. V., ZABUSKY, N. J. & STYCZEK, A. S. 1986 A moment model for vortex interactions of the two-dimensional Euler equations. Part 1. Computational validation of a Hamiltonian elliptical representation. *J. Fluid Mech.* **167**, 95–115.

MIYAZAKI, T. & HANAZAKI, H. 1994 Baroclinic instability of Kirchhoff's elliptic vortex. *J. Fluid Mech.* **261**, 253–271.

MIYAZAKI, T., IMAI, T. & FUKUMOTO, Y. 1995 Three-dimensional instability of Kirchhoff's elliptic vortex. *Phys. Fluids* **7**, 195–202.

MOORE, D. W. & SAFFMAN, P. G. 1971 Structure of a line vortex in an imposed strain. In *Aircraft Wake Turbulence* (ed. J. H. Olsen, A. Goldburg & M. Rogers). Plenum.

PEDLOSKY, J. 1979 *Geophysical Fluid Dynamics*, 2nd Edn. Springer.

POLVANI, L. M. 1991 Two-layer geostrophic vortex dynamics. Part 2. Alignment and two-layer V-states. *J. Fluid Mech.* **225**, 241–270.

POLVANI, L. M., FLIERL, G. R. & ZABUSKY, N. J. 1989 Two-layer geostrophic vortex dynamics. Part 1. Upper-layer V-states and merging. *J. Fluid Mech.* **205**, 215–242.

RHINES, P. B. 1979 Geostrophic turbulence. *Ann. Rev. Fluid Mech.* **11**, 401–441.

SHAPIRO, L. J. & FRANKLIN, J. L. 1994 Potential vorticity in hurricane Gloria. *Mon. Wea. Rev.* **123**, 1465–1475.

STEGNER, A. & ZEITLIN, V. 1995 What can asymptotic expansions tell us about large-scale quasi-geostrophic anticyclonic vortices? *Nonlinear Processes in Geophys.* **2**, 186.

SUTYRIN, G. G., HESTHAVEN, J. S., LYNOV, J. P. & RASMUSSEN, J. J. 1994 Dynamical properties of vortical structures on the beta-plane. *J. Fluid Mech.* **268**, 103–131.

VIERA, F. 1995 On the alignment and axisymmetrization of a vertically tilted geostrophic vortex. *J. Fluid Mech.* **289**, 29–50.

WANG, Y. & HOLLAND, G. J. 1995 On the interaction of tropical-cyclone-scale vortices. IV: Baroclinic vortices. *Q. J. R. Met. Soc.* **121**, 95–126.